



HAL
open science

Geochemical investigation of the taphonomy, stratigraphy, and palaeoecology of the mammals from the Ouled Abdoun Basin (Paleocene-Eocene of Morocco)

Lászl Kocsis, Alex Ulianov, Mustapha Mouflih, Fatima Khaldoune, Emmanuel Gheerbrant

► **To cite this version:**

Lászl Kocsis, Alex Ulianov, Mustapha Mouflih, Fatima Khaldoune, Emmanuel Gheerbrant. Geochemical investigation of the taphonomy, stratigraphy, and palaeoecology of the mammals from the Ouled Abdoun Basin (Paleocene-Eocene of Morocco). *Palaeogeography, Palaeoclimatology, Palaeoecology*, In press, 577, pp.1-17. <10.1016/j.palaeo.2021.110523>. <hal-03269557>

HAL Id: hal-03269557

<https://hal.science/hal-03269557v1>

Submitted on 24 Jun 2021

HAL is a multi-disciplinary open access archive for the deposit and dissemination of scientific research documents, whether they are published or not. The documents may come from teaching and research institutions in France or abroad, or from public or private research centers.

L'archive ouverte pluridisciplinaire **HAL**, est destinée au dépôt et à la diffusion de documents scientifiques de niveau recherche, publiés ou non, émanant des établissements d'enseignement et de recherche français ou étrangers, des laboratoires publics ou privés.



HAL Authorization

32 Marine diagenesis affected the various skeletal tissues differently, with the largest
33 alteration in the bone and the least or none in the enamel. This is mostly demonstrated by
34 the high F concentration, high Ca/P, and seawater related $^{87}\text{Sr}/^{86}\text{Sr}$ in the bone/dentine
35 samples. Enamel shows the opposite, and retained the most pristine terrestrial values. The
36 $\delta^{18}\text{O}_{\text{PO}_4}$ and $\delta^{13}\text{C}$ results from mammal enamel revealed warm ($>20^\circ\text{C}$ mean annual
37 temperature-MAT) and dry ($<500\text{mm}$ mean annual precipitation) conditions for Paleocene-
38 Eocene period in the region. From the early to mid-Ypresian about $+5^\circ\text{C}$ ΔMAT is recorded
39 that might be linked to the Early Eocene Climatic Optimum.

40 Furthermore, the $^{87}\text{Sr}/^{86}\text{Sr}$ ratios derived from shark tooth enameloid fit the global open
41 ocean Sr-isotope record during the latest Paleocene and early Eocene providing further
42 evidence for the age of these phosphate beds in the Ouled Abdoun Basin. However, older
43 marine fossils yielded higher ratios than the global Sr-isotope curve, reflecting an alteration
44 and/or somewhat restricted conditions in the Moroccan coastal basins, possibly triggered by
45 global sea-level changes.

46

47 **Keywords:** bioapatite, rare earth elements, stable isotopes, strontium isotopes,
48 phosphorite.

49

50 **1. Introduction**

51 The phosphate series of the Ouled Abdoun Basin in Morocco, which is exploited in large
52 industrial quarries, is renowned for its Upper Cretaceous-Lower Eocene vertebrate
53 assemblages (e.g., [Arambourg, 1952](#); [Bardet et al., 2017](#)). The fauna predominantly
54 comprises sub-autochthonous marine aquatic organisms such as cartilaginous and bony
55 fishes, mosasaurs, and turtles, but occasionally terrestrial remains have also been described,
56 such as non-avian dinosaurs, birds, and mammals (e.g., [Gheerbrant et al., 2003](#); [Pereda
57 Suberbiola et al., 2004](#); [Bourdon et al., 2005](#)). The mammals are rare and most of the time
58 scientists come to know about them from private collectors living near the phosphate
59 quarries, and often cannot determine their precise stratigraphic origin. Knowing the
60 stratigraphic origins of the Ouled Abdoun fossils is crucial to elucidating the early Cenozoic
61 evolution of African mammals (e.g., [Gheerbrant et al., 2018](#)). Accurate dating of the Ouled
62 Abdoun mammals is also important for knowledge and characterization of the early
63 Cenozoic successive African faunal assemblages.

64 To tackle the stratigraphic origins of vertebrate remains, geochemical taphonomy is a
65 widely used method (e.g., [Staron et al., 2001](#); [Trueman et al., 2003](#); [Metzger et al., 2004](#);
66 [MacFadden et al., 2007](#); [Suarez et al., 2010](#); [Herwartz et al., 2013](#); [Botfalvai et al., 2021](#)).
67 This is based on trace element contents that are absent or occur only in very low
68 concentrations (sub-ppm) in modern bones and teeth, however, after the death of the
69 animals their concentrations increase through the influence of the sedimentary
70 environment (e.g., [Elderfield and Pagett, 1986](#)). The most widely used elements are the rare
71 earths (REE) and uranium, which can reach 4-5 orders of magnitude enrichment in fossil
72 material compared to modern concentrations (e.g., [Trueman and Tuross, 2003](#)). These
73 elements therefore could reflect the chemistry of the pore fluid in which the vertebrate
74 remains were fossilized. There are several studies using REE chemistry of fossil bioapatite to
75 reconstruct palaeoenvironmental conditions in terrestrial and marine depositional settings
76 (e.g., [Trueman et al., 2003](#); [Lécuyer et al. 2004](#); [Shield and Webb, 2004](#); [Kocsis et al., 2009](#);
77 [Žigaitė et al., 2016](#); [2020](#)), which are all based on the assumption that REEs are
78 quantitatively taken up from the burial environment (e.g., [Reynard et al., 1999](#)). During their
79 incorporation into the bioapatite structure, however, fractionation could occur between the
80 light and heavy REEs due to size differences along the REE series and related diffusion (e.g.,
81 [Trueman et al., 2011](#); [Herwartz et al., 2013](#)). In addition, protracted late diagenetic
82 modification ([Kocsis et al., 2010](#); [Herwartz et al., 2011](#)) may further complicate
83 environmental interpretations, especially for older samples ([Kowal-Linka et al., 2014](#)). To
84 address these issues, a large number of samples, including different types of materials (e.g.,
85 bones, teeth, enamel, and dentine), and multiple *in-situ* analyses, are needed to evaluate
86 further the origin of the REEs within the bioapatite.

87 In relation to the Moroccan phosphate series in the Ouled Abdoun and Ganntour basins,
88 the trace element chemistry of nearly 200 marine samples (fish teeth, bones, coprolites)
89 was published in [Kocsis et al. \(2016\)](#). Fractionation and late diagenetic overprint were
90 completely ruled out. All the samples yielded similar, typical oxic seawater REE distributions
91 with heavy REE enrichment and a negative Ce-anomaly. Importantly, however, the Ce-
92 anomalies show a distinct change with stratigraphic level ([Kocsis et al., 2016](#)), a trend that is
93 used in this work to assign a stratigraphic age for unprovenanced fossils. Such an approach
94 was successful for the Embrithopoda mammal taxa of *Stylolophus minor* and *S. major* in the
95 Ouled Abdoun Basin ([Gheerbrant et al., 2018](#)).

96 The main aim of this study is to further investigate the validity of the trace element
97 provenancing method for the rare mammal fossils with known and unknown origins in the
98 Ouled Abdoun Basin. To help better assess the taphonomy of these remains, major and
99 other trace elements, and strontium isotope ratios ($^{87}\text{Sr}/^{86}\text{Sr}$) of selected mammal fossils,
100 were compared with marine end-members such as data from shark teeth. Enameloid
101 $^{87}\text{Sr}/^{86}\text{Sr}$ data derived from the latter also provide a proxy for the age of the phosphate
102 beds, through comparing their ratios with the global $^{87}\text{Sr}/^{86}\text{Sr}$ record. In addition, some
103 mammal fossils were measured for their stable oxygen and carbon isotopic compositions to
104 get an insight into the ecological conditions of some of these early African placental
105 mammals.

106

107 **2. Geological and stratigraphical settings**

108 The Ouled Abdoun Basin is one of the ancient epicontinental marine basins along the
109 Atlantic coast of Africa, where large amounts of phosphorite accumulated during the late
110 Cretaceous - early Eocene period. The basement rocks are covered by Cenomanian-Turonian
111 carbonates followed by yellow marls with possible age within the Coniacian-Campanian
112 interval ([El Assel et al., 2013](#)), which were eventually succeeded by the phosphorite series.
113 The top of the succession is either covered by Lutetian dolomitic limestone or by Neogene
114 continental beds ([OCP, 1989](#)). In the phosphorite series, three sequences (A-C) of 2nd order
115 transgressive-regressive (T-R) cycles ([Vail et al., 1991](#)) are recognized, with ages of
116 Maastrichtian (latest Cretaceous) (A), Danian-Thanelian (Paleocene) (B), and Ypresian (early
117 Eocene) (C). These T-R cycles are further divided into 3rd order cycles that begin with P-rich
118 phosphate (often granular in appearance), and end with clayey, carbonate, or siliceous
119 deposits. The phosphorite series is often followed by a fourth sequence (D) but without
120 phosphate occurrences ([EL Haddi, 2014](#)), marking the reduction of phosphogenesis and the
121 installation of silicified limestone with lumachellic texture and the occurrence of Thersitea-
122 type gastropods ([Mouflih, 2015](#)).

123 Regional correlation and biostratigraphy of these sediments are achieved by examining
124 selachian remains (i.e., shark and ray teeth), which are extremely abundant (e.g.,
125 [Arambourg, 1952](#); [Noubhani and Cappetta, 1997](#); [Cappetta et al., 2014](#)), while other, non-
126 phosphatic fossils are either very poorly preserved or do not have significant stratigraphic
127 value (e.g., [Ollivier-Pierre, 1982](#); [Rauscher, 1985](#); [Soncini, 1990](#)). Chemostratigraphy based

128 on the $\delta^{13}\text{C}$ of residual organic matter (Yans et al., 2014) and the $\delta^{18}\text{O}$ and $\delta^{13}\text{C}$ of marine
129 vertebrate fossils (Kocsis et al., 2014a), however, revealed some details about the timing of
130 the Paleogene beds such as (1) sedimentation occurred during the middle Paleocene
131 (Selandian, 61.5-59.2 Ma); (2) a possible lack of sedimentation during the latest Paleocene
132 (late Thanetian, ~57-56 Ma), probably including the Paleocene-Eocene Thermal Maximum
133 (PETM); and (3) the third sequence (C) was deposited during the early Eocene (early - ?late
134 Ypresian, ~56-51 Ma) including the Early Eocene Climatic Optimum (EECO).

135 Traditionally, the phosphate succession in the Ouled Abdoun Basin is further subdivided
136 into several phosphate-rich beds of industrial value (from base to top, beds III, II, I, 0) with
137 the non-exploited horizons of calcareous phosphate, chert, or thin clay between them called
138 intercalary beds (Figure 1). Bed III refers to the Late Cretaceous layers, Bed IIa and Bed IIb to
139 the Paleocene beds, while Bed I, Bed 0', Bed 0, and the top layers called "sillons" are early
140 Eocene, as determined from the associated selachian faunas (Arambourg, 1952; Noubhani
141 and Cappetta, 1997) (Figure 1). Upsection the proportions of phosphate decrease and chert-
142 rich sediments occur more often. The successive phosphate beds recurrently enclose "bone
143 beds" where vertebrate remains are concentrated, probably as a result of hydrodynamic
144 accumulations and/or during a period of condensation of bioclastic material with a low
145 sedimentation rate (Gheerbrant et al., 2003). Three of them also yielded unique mammal
146 remains: (1) the *Eritherium* bone bed at the base of Bed IIa, dated Selandian (61.6 - 59.2
147 Ma); (2) the big coprolite bone bed in the upper part of Bed IIa, dated Thanetian (59.2-56
148 Ma); and (3) the earliest Ypresian (~56-55 Ma) *Otodus obliquus* bone bed within intercalary
149 bed II/I (Figure 1). Mammals also derived from two younger levels (Figure 1) such as (4) the
150 base of Bed I, dated lower Ypresian (~55-54 Ma); and (5) the upper phosphate horizons, Bed
151 0 and the "sillons", dated middle Ypresian (~53-51 Ma) (Yans et al., 2014; Kocsis et al.,
152 2014a).

153 The mammals recovered from these Paleocene and lower Eocene phosphate beds are
154 the earliest known placentals in Africa, together with those from the Ouarzazate Basin
155 (Gheerbrant et al., 2017). Despite their rarity, they document an unexpected taxonomic
156 diversity, especially for paenungulates (Afrotheria), which comprise 7 genera and 10 species
157 (*Abounodus*, *Ocepeia daouiensis*, *O. grandis*, *Eritherium*, *Phosphatherium*, *Daouitherium*,
158 *Seggeurius*, Paenungulata indet., *Stylolophus minor*, *S. major*; see Gheerbrant et al., 1998,
159 2001, 2003, 2009, 2014, 2018; Bardet et al., 2017).

160

161 **3. Material and Methods**

162 *3.1. Investigated materials*

163 Several mammal species and/or other fossils from the mammal-related sediment matrix
164 were involved in our research. Some of the fossils have known stratigraphic positions, while
165 the origins of the others are questionable or completely unknown (Table 1). We focused
166 primarily on the trace element compositions of the fossils (Table 1). However, some
167 specimens were also analyzed for the presence of major elements (Ca, P, F), stable oxygen
168 and carbon isotopes, and radiogenic strontium isotopes. The latter taxa are *Daouitherium*
169 *rebouli* (Bed 0), *Phosphatherium escuilliei* (intercalary Bed II/Bed I, and Bed I), Hyracoidea
170 indet (unknown bed; Gheerbrant et al., 2003), *Ocepeia grandis* (Bed IIa; Gheerbrant et al.,
171 2014), and *Eritherium azzouzorom* (base of Bed IIa, i.e., *Eritherium* bone bed). These
172 mammals are mostly known by fragments of jaws and, in the best cases, by a few skulls, and
173 all of them are early representatives of the African endemic placental ungulates
174 (Paenungulata). In particular *Eritherium* (Gheerbrant, 2009, Gheerbrant et al., 2012),
175 *Phosphatherium* (Gheerbrant et al., 2005), and *Daouitherium* (Gheerbrant et al., 2002) are
176 the earliest and most basal proboscideans. They document the very early emergence in
177 Africa of one of the most remarkable lineage of extant placentals, the elephant order
178 (Gheerbrant, 2009).

179 Often different parts have been analyzed and compared in parallel, such as mammal
180 tooth enamel and dentine, bone, and – from the sediment matrix – shark tooth enameloid,
181 dentine, and coprolites. More details about the analyses of these are presented in the
182 Methods section.

183 In addition, the background trace element dataset (Kocsis et al., 2016) is extended here
184 by samples analyzed from the big coprolite bone bed (upper part of Bed IIa) from quarries of
185 Sidi Chennane (N32°38'25", W6°43'22") and Sidi Daoui (Meraa El Arech Nord - N32°46'47",
186 W6°45'4"), while a few specimens from the *Eritherium* and *Otodus obliquus* bone beds were
187 also added from Sidi Daoui near Meraa El Arech Nord and Boujniba (N32°52'16",
188 W6°47'13"), respectively (Supplementary Material Table-1).

189

190 *3.2. Major and trace element compositions*

191 All the analyses were carried out at the Institute of Earth Sciences, University of
192 Lausanne, Switzerland. The mammal remains (teeth and bones) and fossils from the
193 associated matrix (fish teeth, coprolites) were cut with a micro-saw, then small pieces were
194 embedded in epoxy resin and flat-polished. The major-element contents of selected fossils
195 were determined by using wavelength-dispersive analysis with a JEOL 8200 microprobe. The
196 concentrations of rare earth and other trace elements were measured by Laser Ablation-
197 Inductively Coupled Plasma-Mass Spectrometry (LA-ICP-MS), using a GeoLas 200M ArF
198 excimer laser (193nm) coupled to a Perkin-Elmer ELAN 6100 DRC quadrupole spectrometer
199 or via Element XR ICP-MS with a linked RESOLUTION ablation system. The ablation was carried
200 out in a He atmosphere using spot sizes of 60-80 μm in diameter. Standard reference
201 materials 612 from NIST, representing silica-lime-alumina glasses doped with trace
202 elements, were used for external standardization (Pearce et al., 1997). ^{42}Ca was analyzed as
203 an internal standard; CaO values of 54, 51 and 50 wt.% were used respectively for shark
204 tooth enameloid, mammal enamel, and for more porous material such as dentine, bone and
205 coprolites. These values are the overall average CaO content of the different remains
206 derived from the microprobe data presented here (Supplementary Material Table-2) and
207 provided in Kocsis et al. (2014a). The analytical reproducibility was generally better than
208 $\pm 5\%$ SE.

209

210 3.3. Strontium isotope ratios ($^{87}\text{Sr}/^{86}\text{Sr}$)

211 The chemical separation of Sr and mass spectrometry were performed at the
212 Department of Earth Sciences, University of Geneva (Switzerland). Selected fossils were
213 cleaned in an ultrasonic bath to reduce any sedimentary contamination, then the external
214 0.5-1 mm surface was removed that might have been altered in the depositional
215 environment. From the cleaned surface about 2-5 mg of mammal enamel(oid) / dentine /
216 bone powder was obtained using a micro-drill, and was dissolved in Teflon beakers at 80°C
217 in 2M HCl. Sr separation was performed by extraction chromatography using Eichrom's Sr-
218 Spec resin according to a protocol modified from Pin et al. (1994). Strontium was analysed in
219 2% HNO_3 solution on a Neptune Plus Multi Collector ICP-MS. Interferences at masses ^{84}Sr
220 (^{84}Kr), ^{86}Sr (^{86}Kr) and ^{87}Sr (^{87}Rb) were corrected by monitoring ^{83}Kr and ^{85}Rb . Mass
221 fractionation was internally corrected assuming a $^{88}\text{Sr}/^{86}\text{Sr}$ ratio of 8.375209. The values
222 were internally corrected further for external fractionation based on repeat analyses of the

223 strontium NBS 987 standard (nominal value of 0.710248), which yielded an average $^{87}\text{Sr}/^{86}\text{Sr}$
224 value of 0.710270 (10 ppm long-term reproducibility, 1σ).

225

226 3.4. Stable isotope analyses ($\delta^{18}\text{O}_{\text{PO}_4}$, $\delta^{13}\text{C}$, $\delta^{18}\text{O}_{\text{CO}_3}$)

227 The sample preparation and analyses were performed in the Stable Isotope Laboratory
228 of the Institute of Earth Surface Dynamics at the University of Lausanne, Switzerland.
229 Sample preparation and some of the analytical backgrounds are summarized in [Kocsis et al.](#)
230 [\(2014a\)](#). The oxygen isotope composition of PO_4^{3-} ion was analysed with a high-temperature
231 conversion elemental analyser (TC/EA) coupled to a Finnigan MAT Delta Plus XL mass
232 spectrometer. The results were corrected to in-house Ag_3PO_4 phosphate standards (LK-2 L:
233 12.1‰ and LK-3 L: 17.9‰) with better than $\pm 0.3\%$ (1σ) standard deviations during the runs.
234 NBS-120c phosphorite reference material was prepared in parallel with the samples and an
235 average value of $21.6 \pm 0.3\%$ ($n = 10$) was obtained. The carbon and oxygen isotope
236 compositions of the structural carbonate in the apatite were analysed with a Gasbench II
237 coupled to a Finnigan MAT Delta Plus XL mass spectrometer. The measured isotopic ratios
238 were normalized to an in-house Carrara marble calcite standard that is calibrated against
239 NBS-19. The analytical precision for this method is better than $\pm 0.1\%$ for O and C isotopes.
240 The data are expressed in delta notation, in the case of $\delta^{18}\text{O}_{\text{PO}_4}$ relative to VSMOW (Vienna
241 Standard Mean Ocean Water), while the $\delta^{13}\text{C}$ and $\delta^{18}\text{O}_{\text{CO}_3}$ results from the structural
242 carbonate analyses are shown relative to VPDB (Vienna Pee Dee Belemnite).

243

244 4. Results

245 4.1. Major element compositions

246 The remains of four mammal taxa, *Daouitherium rebouli* (PM65), *Phosphatherium*
247 *escuilliei* (MNHN.F PM25), Hyracoidea indet (MNHN.F PM52), and *Ocepeia grandis* (PM66)
248 were analyzed for CaO, P_2O_5 and F content ([Table 2](#), [Figure 2](#)). The Ca/P ratio ranges from
249 1.70 to 2.02, with the values increasing from enamel to dentine to bone. The F content
250 varies between 0.73 and 3.95 wt% and a similar trend to the Ca/P ratio can be seen, as the
251 lower values come from the enamel, and the highest ones from the bone samples ([Figure 2](#)).

252

253 4.2. Trace element compositions

254 Nineteen mammal specimens, sometimes represented by several different parts (tooth
255 enamel, dentine, and bone fragments) and/or related sediment matrix elements (coprolites,
256 fish teeth), were involved in the trace element study. Often multiple fragments of the same
257 individual together with dentine-enamel pairs were analyzed and considered separately.
258 The stratigraphic origin of each mammal specimen (i.e., the layer it comes from), therefore
259 is represented by between one and eight sub-samples (see [Table 1](#)). Each of these
260 represents the average of 1 to 4 spot analyses ([Table 2](#)). Altogether, 67 sub-samples were
261 analyzed, of which 32 are directly from mammal remains, while the rests are from sediment
262 matrix elements related to the mammals. Prior study indicates that samples from the same
263 layers yielded a similar REE distribution ([Kocsis et al., 2016](#)), and hence unique mammal
264 fossils (e.g., types specimens) not available for sampling can be represented by geochemical
265 data analyzed from the matrix elements in the sediments attached to these rare fossils.

266 The trace element concentration data and ratios are listed in Supplementary Material
267 Table-3, and selected ones are plotted in [Figures 3-5](#). A range of elements, such as Sr, Zn, Ba,
268 totREE and U, are compared in the boxplots ([Figure 3](#)). Sr is especially enriched in the shark
269 tooth enameloid (average > 2035 ppm), while other types of remains hardly reach 1000
270 ppm. On average, the zinc concentration is somewhat higher in the enamel and enameloid,
271 while barium is more enriched in the terrestrial remains. Variations of the early diagenetic
272 rare earth elements (REE) and U concentrations within the samples are similar to data
273 already reported from the Ouled Abdoun Basin ([Kocsis et al., 2016](#)). For example, the denser
274 enamel/enameloid generally yielded lower concentrations compared to dentine, bones or
275 coprolites. Importantly, all the investigated specimens, the mammals and the marine matrix
276 elements, show very similar REE patterns with a negative Ce-anomaly and heavy REE
277 enrichment. The Ce-anomaly and the Pr-anomaly can be quantified as $Ce/Ce^* = 2Ce_N /$
278 $(La_N + Pr_N)$ and $Pr/Pr^* = 2 Pr_N / (Ce_N + Nd_N)$, where N denotes the Post-Archean Australian
279 Shale (PAAS) normalized value ([McLennan, 1989](#)). These parameters, however reveal subtle
280 variations among the samples, as they link to stratigraphic origin rather than taxon
281 affiliation ([Figures 4-6](#)).

282

283 4.3. Strontium isotope ratios ($^{87}Sr/^{86}Sr$)

284 Four mammal specimens from different ages were chosen and altogether nine separated
285 analyses were carried out: four enamel, three dentine and two bones ([Table 2, Figure 7](#)).

286 The $^{87}\text{Sr}/^{86}\text{Sr}$ ratios vary between 0.707856 and 0.708182, and a clear decreasing trend from
287 enamel through dentine to bones is observed. In addition, twenty-four shark tooth
288 enameloids - 16 from the Ouled Abdoun Basin and 8 from the nearby Ganntour Basin - were
289 measured for $^{87}\text{Sr}/^{86}\text{Sr}$ ratios, and yielded a range from 0.707714 to 0.707920
290 (Supplementary Material Table-5). The data are shown in [Figure 7](#), together with a
291 comparison to the global strontium evolution curve for the open ocean (see [McArthur et al.,](#)
292 [2020](#)).

293

294 4.4. Stable isotope analyses ($\delta^{18}\text{O}_{\text{PO}_4}$, $\delta^{13}\text{C}$, $\delta^{18}\text{O}_{\text{CO}_3}$)

295 Ten mammal specimens from five taxa (*D. rebouli*, Hyracoidea indet., *P. escuilliei*, *O.*
296 *grandis*, *E. azzouzorom*; [Table 2](#)) were analysed for phosphate oxygen isotopic composition,
297 chiefly in the tooth enamel, but a few dentine and bone samples were analysed as well. No
298 systematic variation was observed among these materials. The $\delta^{18}\text{O}_{\text{PO}_4}$ data vary between
299 18.0 and 22.6 ‰ and the overall average value is 19.8 ± 1.1 ‰ (n = 19). Individual mean
300 values and taxon averages are shown in [Table 2](#), while the taxon-related variation is plotted
301 in [Figure 8](#). One of the *Daouitherium rebouli* specimens (MNHN.F PM3) yielded the highest
302 $\delta^{18}\text{O}_{\text{PO}_4}$ value (22.3 ± 0.4 ‰, n = 2), while the other specimens (PM65, ML 20269987) of this
303 species vary between 18.6 and 21.2 ‰. Only eight samples were analyzed for isotopic
304 composition in the structural carbonate in the bioapatite ($\delta^{13}\text{C}$, $\delta^{18}\text{O}_{\text{CO}_3}$), belonging to four
305 taxa. The $\delta^{13}\text{C}$ derived enamel (n = 5) ranged between -7.1 and -8.6 ‰, while a dentine and
306 two bone samples yielded higher values of -6.3, -4.6, and -3.9 ‰, respectively ([Table 2](#),
307 [Figure 8](#)). The values of $\delta^{18}\text{O}_{\text{CO}_3}$ ranged between -3.7 and -5.1 ‰ for the enamel, whereas
308 the dentine and the two bones yielded somewhat lower values of -5.6, -5.6, and -5.1 ‰,
309 respectively ([Table 2](#)).

310

311 5. Discussion

312 5.1. Terrestrial, marine, and diagenetic signals

313 Hard tissues (i.e., bones, teeth) of terrestrial and marine animals record the chemical and
314 isotopic signatures of their respective environments, hence when these remains are
315 fossilized the ancient ecological conditions can be traced in the case of no alteration (e.g.,
316 [Tütken et al., 2006](#); [Kocsis et al., 2007](#); [Domingo et al., 2009](#); [Reynard and Balter, 2014](#);

317 Akhtar et al., 2020). Generally, freshwater (e.g., terrestrial drinking sources) has a lower F
318 and Sr content than seawater, while Ba is instead expected to be higher in rivers and lakes
319 (White 1998; Bruland and Lohan 2003; Gaillardet et al. 2003). Therefore, these elements can
320 help tracing *in-vivo* preserved environmental signals, and can give information on alteration
321 during fossilization. Moreover, the taphonomic relations of mixed assemblages, such as the
322 one studied here, can be further investigated (e.g., Trueman et al., 2003; Tütken et al.,
323 2008).

324 In this study, the low F and high Ba content, but also the low Ca/P and high $^{87}\text{Sr}/^{86}\text{Sr}$
325 ratios in the mammal tooth enamel, indicate at least partially preserved *in-vivo* values
326 reflecting a continental source and origin. The higher F and lower Ba concentrations, and Sr-
327 isotope ratios in the mammal dentine and bone that are closer to marine values, are best
328 explained by diagenesis in a seawater-dominated pore fluid (Figures 2-3). The burial
329 condition is also reflected by the chemistry of the marine coprolites (Figure 2), which
330 phosphatized within the sediments (Cosmidis et al., 2013), and yielded similar compositions
331 to those of the mammal bones and dentine. Therefore, the Ca/P ratio and F of these
332 mammal remains were altered in a marine depositional setting. The latter materials have a
333 higher susceptibility to interaction and exchange with the depositional fluid due to their
334 lower crystallinity and density, and originally higher porosity and organic content when
335 compared to the enamel. The higher concentrations of REE and U, and possibly the higher
336 $\delta^{13}\text{C}$ and lower $\delta^{18}\text{O}_{\text{CO}_3}$ values, in the dentine and bone are also the result of the postulated
337 structural differences and related diagenesis in a marine pore-fluid (Figure 3 & 8, Table 2).

338 As an *in-vivo* marine environmental end-member, shark tooth enameloid is the best
339 suited material, as it is indicated by the following geochemical data: (1) a high F content, (2)
340 low Ca/P ratios, (3) a high Sr concentration, and (4) very similar $^{87}\text{Sr}/^{86}\text{Sr}$ ratios to the open
341 seawater of the time (McArthur et al., 2020; see chapter 5.3), and partly also (5) oxic-
342 seawater related REE patterns (Figure 4; Kocsis et al., 2016) (Figure 2).

343 Based on the above observations, enamel/enameloid geochemical values should be used
344 in any ecological and *in-vivo* interpretations. In this sense, the somewhat higher
345 concentrations of Zn in both the mammal enamel and shark tooth enameloid call for further
346 explanation, as these values may link to a common *in-vivo* origin. Zn has been connected to
347 enzymes (e.g., kallikrein - KLK4) that play an important role in mammal tooth enamel
348 formation (amelogenesis). In fact, KLK4 helps in removing organic matter at a later stage, so

349 as to make the enamel harder (e.g., [Simmer et al., 2009](#); [Goetttig et al., 2010](#)). A high Zn
350 concentration has been detected in modern shark enameloid and a similar enzymatic
351 process has been proposed ([Kocsis et al., 2015](#)). Therefore, the observed relatively higher Zn
352 concentration in our enamel/enameloid may partly relate to the process of enamel
353 mineralization during amelogenesis. For other *in-vivo* interpretations based on the stable
354 isotope and strontium isotope ratios, see Sections 5.3 and 5.4.

355

356 5.2. REE element taphonomy and stratigraphy

357 The rare earth element content of fossil bioapatite is predominantly of early diagenetic
358 origin and can reflect the burial fluid's REE composition (e.g., [Elderfield and Pagett, 1986](#);
359 [Trueman and Tuross, 2002](#)). This signature of fluid composition is frequently used to address
360 taphonomic questions related to fossil vertebrates (e.g., [Staron et al., 2001](#); [Trueman et al.,](#)
361 [2003](#); [MacFadden et al., 2007](#); [Tütken et al., 2008](#); [Botfalvai et al., 2021](#)) or to assess
362 palaeoenvironmental conditions (e.g., [Picard et al., 2002](#); [Shield and Webb, 2004](#); [Kocsis et](#)
363 [al., 2007, 2009](#); [Žigaitė et al., 2016, 2020](#)). From the Ouled Abdoun and Ganntour basins in
364 Morocco, [Kocsis et al. \(2016\)](#) tested over 200 bioapatite specimens, and this database has
365 been extended here (Supplementary Material Table-1). Based on the REE concentrations,
366 their variations along the phosphate series, and their variations within the specimens, any
367 late diagenetic overprint or fractionation along the REE series is ruled out (e.g., [Kocsis et al.,](#)
368 [2016](#)). Therefore, the REE patterns we have obtained, and the related elemental ratios, can
369 confidently be linked to the depositional environment.

370 As was the case in the prior study, the REE content of the fossils analyzed here increases
371 from enamel/enameloid to coprolite, dentine, and bone, which, as mentioned earlier,
372 reflects original structural and compositional (i.e., organic content) differences among these
373 materials. However, a very important fact is that all the samples (in this study and in [Kocsis](#)
374 [et al. 2016](#)), yielded similar REE distributions, which mimic oxic seawater patterns (i.e., a
375 negative Ce-anomaly and HREE enrichment) regardless of the material and taxa involved
376 ([Figure 4](#)). This further supports the conjecture that the terrestrial mammal remains were
377 fossilized within a marine depositional setting together with the marine fossils, and that
378 they gained their REE content from seawater dominated pore fluids. An additional
379 implication is that the mammal carcasses were most likely directly transported into the
380 marine realm, without any previous terrestrial depositional site in the hinterland. This is

381 compatible with the hypothesis that the terrestrial mammals were drained as floated bodies
382 from the nearby hinterland by local rivers in the Ouled Abdoun phosphate basin, shortly
383 after their deaths (Gheerbrant et al., 2003).

384 Despite the very similar REE patterns, the samples do vary in their Ce/Ce* and Pr/Pr*
385 ratios, which together express the degree of Ce-anomaly (Figure 4) (Bau and Dulski, 1996).
386 The variations in the ratios are time related, meaning that samples from the same bed
387 cluster around similar values. Therefore the REE distribution of any remains from the
388 sediment matrix, such as coprolites, pellets or small teeth, attached or embedded with the
389 mammal fossils, represents these rare fossils with no bias (see Table 1).

390 The few mammal samples and/or their sediment matrix whose stratigraphic origins were
391 previously known perfectly match the reference Ce/Ce* curve established by Kocsis et al.
392 (2016) (Figure 5). Moreover, taxa with presumably Paleocene (e.g., Ocepeiidae spp.,
393 *Abdounodus*, *Eritherium*) or Eocene (e.g., *Phosphatherium*, *Daouitherium*, *Stylolophus* spp.)
394 ages fit in the corresponding data cluster (Figure 4).

395 The background Ce/Ce* dataset for the Ouled Abdoun Basin allows for comparison of the
396 mammal-derived data with their possible stratigraphic positions (Figures 4-6). The
397 sedimentary section was divided into ten chemostratigraphic horizons based on the Ce/Ce*
398 variation and major sedimentological units including the three bone-beds (Horizons 3, 5,
399 and 7), where mammal remains presumably were found. The variance and mean of the
400 Ce/Ce* values for the consecutive layers were compared using the F and Student's-t tests
401 respectively (Supplementary Material Table-6), and these yielded significant differences
402 (Student's t-test $p < 0.05$) with the exceptions of the top of Bed-IIb (Horizon 8) and the
403 *Eritherium* bone bed (Horizon 7) ($p = 0.604$). Then, in order to trace the possible
404 stratigraphic origin of the mammals, each mammal data-group ($n > 2$) was compared to the
405 respective horizons using one-way ANOVA (i.e., Eocene mammals to Horizons 1 - 5;
406 Paleocene mammals to Horizons 5 - 10), and the underlying differences in the mean Ce/Ce*
407 values were checked using Tukey's pairwise tests (Table 3).

408

409 5.2.1 Paleocene taxa

410 The three specimens of *Eritherium azzouzorum* (PM40; MNHN.F.PM42; PM100a see
411 Table 1) found in the *Eritherium* bone bed fit the background Ce/Ce* data from this horizon
412 (Horizon 7). However, they are also statistically similar to the horizons below and above. The

413 Ce/Ce* data of the taxa with unknown provenance revealed that their origin is restricted to
414 the interval between the very top of Bed IIb and the base of Bed IIa, including the *Eritherium*
415 bone bed (chemostratigraphic Horizons 6-8 i.e., early Thanetian–Selandian–?latest Danian
416 age)(Figure 6, Table 3). This suggests that these mammal specimens do not come from
417 younger Paleocene bone beds such as the big coprolite bone bed (base of Horizon 5), which
418 was the suspected provenance of one of the *O. grandis* specimens (PM66) based on
419 information from local collectors. Fossil collectors usually target higher accumulations of
420 bones (i.e., the bone beds) to find unique specimens, hence the *Eritherium* bone bed
421 (Horizon 7) could be the most important source of these fossils. However, our results
422 support the hypothesis that some mammal specimens such as MNHN.F PM39 of *O. grandis*,
423 – and solely based on its Ce/Ce* ratio – maybe even the MNHN.F PM42 of *E. azzouorum*,
424 might be derived from layers overlying the base of Bed IIa (Horizon 6) (Figure 6). Among the
425 Ocepeiidae, the overlapping probabilities of their stratigraphic provenance indicate that the
426 smaller *O. daouiensis* and the larger *O. grandis* were co-existing, therefore refuting the
427 possibility that they were successive chronospecies (Table 3-4, Figure 5). For the specimens
428 where only one Ce/Ce* data point is available (Ocepeiidae? – MHNM.KHG.224 and
429 *Abdounodus hamdii* - PM67), the result agree with the suggested origin in Horizons 6-8.

430

431 5.2.2 Eocene taxa

432 The Eocene taxa reveal a wider range of possible provenance beds, based on the
433 statistical analysis (Table 3). This relates partly to the fact that the Ce/Ce* values are
434 increasing in the youngest beds, and so they overlap with some of the older levels, while the
435 latest Paleocene beds (top Bed IIa – Horizon 5) show very similar values to those of the early
436 Ypresian beds (Figure 5). An exception is Horizon 4, with few specimens (the very base of
437 intercalary II/I), which clearly does not match any of the taxa due to its high Ce/Ce* values,
438 and which are similar to the older Paleocene data series. This small spike in the Ce/Ce*
439 values may reflect reworked older specimens from Bed IIa, as has been recognized also by
440 Gheerbrant et al. (2003), and/or a very brief episode of less oxic, somewhat confined
441 conditions (probably after the PETM event) (Kocsis et al., 2016).

442 On the other hand, most of the taxa show significant undifferentiated similarities to the
443 whole range of chemostratigraphic Horizons 1, 3, and 5, i.e. upper Thanetian-Ypresian
444 (Figure 6). Unfortunately, the Ce/Ce* chemostratigraphic approach alone could not help to

445 define the exact provenance of the mammal taxa in these three horizons, so additional
446 information from the sediment matrix and related selachian fauna (i.e., shark and ray) are
447 needed for further stratigraphic assignment.

448 The origin of the few *Phosphatherium escuilliei* specimens (MNHN.F PM14 and MNHN.F
449 PM17) is known for certain to be the *Otodus obliquus* bone bed in the intercalary phosphate
450 Beds II/I (i.e., base Horizon 3) (Table-1, Gheerbrant et al., 2005), but no trace element
451 analyses were carried out on these specimens. However, the specimens of this species with
452 unknown provenance (MNHN.F PM25, OCP DEK/GE336) yielded Ce/Ce* data fitting an
453 origin in Horizon 3, which includes the *Otodus obliquus* bone bed (Figure 6).

454 The sediment matrix and the related selachian remains assigned the *Stylolophus minor*
455 (OCP DEK/GE 668) specimen to the *Otodus obliquus* bone bed, a conclusion which is further
456 confirmed by its Ce/Ce* values (Figure 5). Selachian taxa found in the matrix of the other
457 specimen of *S. minor* (MNHN.F PM30) are also compatible with Horizon 3 (see
458 Supplementary Material Table-7). The Ce/Ce* data for the other specimens analyzed
459 (MNHN.F PM30 & OCP DEK/GE 667) would also match an origin in Horizon 3 (early Ypresian)
460 (Figure 6).

461 For these two species (*P. escuilliei* and *S. minor*), however, the general similarity in the
462 Ce/Ce* values to the latest Paleocene beds (Horizon 5: top Bed IIa including the big
463 coprolite bone bed) raise the possibility that some of these specimens may have belonged
464 to the older Horizon 5. Thus, we cannot exclude that these species have crossed the PETM
465 boundary. It must be mentioned that the provenance of *P. escuilliei* and *S. minor* from
466 Horizon 1 (Table 3) is completely rejected here, due to the lack of strong similarities with the
467 thick succession of Horizon 2, which stratigraphically follows Horizon 3 (Figure 5).

468 *Stylolophus major* (MNHN.F PM53) has the highest probability of occurrence in the
469 youngest Horizon 1 (the sillons beds – Table 3, Figure 6). If it is correct, it would be the
470 stratigraphically youngest mammal recovered in the Ouled Abdoun phosphate series. A
471 stratigraphic origin of *S. major* from the sillons beds is further supported by its larger size
472 and its more derived morphology with respect to *S. minor*, and also by the chert content
473 and the selachian assemblage found in its matrix (Gheerbrant et al., 2018, 2020). In fact, this
474 species yielded very different Ce/Ce* and Pr/Pr* ratios from the rest of the mammals (see
475 Figure 4d), and when Tukey's pairwise comparison is applied to all these younger taxa it
476 reveals that *S. major* is significantly different from the rest of the remains ($p < 0.05$, Table 4),

477 which further supports its younger origin in the phosphate series (i.e., Horizon 1 – late
478 Middle Ypresian).

479 For *Daouitherium rebouli*, the matrix data and related fauna suggest an origin in Bed 0 or
480 Bed 0' (Horizon 2) (see Supplementary Material Table-7). Generally, our Ce/Ce* data
481 support this scenario, although Horizons 1 and 3 yielded a higher probability match.
482 Moreover, these specimens do not differ in their Ce/Ce* values from those of *P. escuilliei*
483 and *S. minor* (Table 4). The Ce/Ce* data match Horizon 5 (Paleocene), but the attached
484 matrix-type and related selachian fauna preclude this scenario (see Table 3). *Daouitherium*
485 is the largest proboscidean from the Ouled Abdoun Basin and most probably evolved
486 somewhat later than *Phosphatherium*, so the younger age might be possible too
487 (Gheerbrant et al., 2002). Here we propose an origin in the interval from the top Horizon 3
488 to Horizon 2 (middle Ypresian) (see the grey shaded area in Figure 5).

489 The difficulties in pinpointing more precise stratigraphic provenances based on only the
490 Ce/Ce* data is clear from the above example, and the limitations of the method are further
491 highlighted by the Hyracoidea specimen (MNHN.F PM52), for which no additional matrix
492 related information is available. The similar probability pattern to the *D. rebouli* specimens
493 (Table 3) may suggest a similar origin; while significant differences from the holotype of *S.*
494 *major* (Table 4) would argue against a provenance in Horizon 1. Therefore, we propose here
495 a possible origin for the Hyracoidea from the top of Horizon 3 to Horizon 2 (middle
496 Ypresian).

497

498 To sum up, in general the chemostratigraphic approach supports the previous
499 assumptions made about the provenances of the mammal taxa investigated here, but it has
500 also shed light on certain peculiarities such as (1) the Ocepeiidae species, in particular *O.*
501 *daouiensis* and *O. grandis*, coexisted in the Ouled Abdoun phosphate series for an
502 undetermined period from the latest Danian to the early Thanetian; (2) the Ypresian species
503 *P. escuilliei* and *S. minor* might have already evolved in the latest Paleocene; (3) *Stylolophus*
504 *major* is the youngest and only known mammal taxon derived from the highest phosphorite
505 sillon beds (late Middle Ypresian). Based on the Ce/Ce* data and additional matrix and
506 biostratigraphic (i.e., selachian fauna) information, the most probable stratigraphic origin of
507 the mammal specimens are marked by the grey areas in Figure 6.

508

509 5.3. Strontium isotope ratios in terrestrial and marine fossils

510 The Sr that is biologically available in a terrestrial environment is affected by the local
511 geology, and it is incorporated into the skeletal tissues via ingestion without fractionation
512 along the food chain (e.g., Blum et al., 2000). Therefore, the strontium isotope ratios
513 ($^{87}\text{Sr}/^{86}\text{Sr}$) of fossil terrestrial mammals are often used to trace migration patterns (e.g.,
514 Hoppe et al., 1999; Tütken et al., 2006; Arppe et al., 2009). On the other hand, in the open
515 marine realm the seawater has a constant $^{87}\text{Sr}/^{86}\text{Sr}$ ratio due to the long residence time of
516 Sr. However, on longer timescale the ratio does vary, and this variation is the basis of
517 strontium isotope stratigraphy (e.g., McArthur et al. 2020). Dating marine rocks with well-
518 preserved fish remains is one widely used approach (e.g., Ingram 1995; Kocsis et al., 2013;
519 Harrell et al., 2016), while in the case of mixed terrestrial and marine assemblages,
520 taphonomy of the remains can give further information.

521 Our $^{87}\text{Sr}/^{86}\text{Sr}$ analyses from the Ouled Abdoun basin yielded differences between the
522 continental and marine taxa, with the mammal fossils in general having higher ratios (Figure
523 7a). The highest ratios come from mammal enamel that represents possibly unaltered
524 terrestrially-derived and ingested Sr (i.e., *in-vivo*), which reflects the hinterland geology of
525 the time. The $^{87}\text{Sr}/^{86}\text{Sr}$ ratios decrease through dentine to the bone samples, which
526 approaches the values of the open ocean (Figure 7a). This decreasing trend within the
527 different types of mammal remains clearly indicates diagenesis in a marine depositional
528 environment, and as mentioned earlier this has an important taphonomic message. The
529 remains were originally deposited in a marine setting and they are not reworked from
530 previous deposits.

531 On the other hand, the data derived from the shark tooth enameloid more or less follow
532 the global open ocean Sr-evolution curve. This is most noticeable for the latest Paleocene
533 and Eocene where the Sr-isotope ages agree with other chemostratigraphic data (Yans et
534 al., 2014; Kocsis et al., 2014a). However, the rest of the Paleocene and part of the
535 Cretaceous samples yielded $^{87}\text{Sr}/^{86}\text{Sr}$ ratios that cannot fit the global Sr-isotope curve
536 because their values are too high (Figure 7). The most plausible interpretation is that these
537 samples were altered during early diagenesis. A high $^{87}\text{Sr}/^{86}\text{Sr}$ ratio could have derived from
538 a terrestrial source, as attested by the mammal enamel's high $^{87}\text{Sr}/^{86}\text{Sr}$ values. However,
539 there is no evidence of strong continental input in the sedimentary record of the
540 phosphates series, which corresponds mostly to non-clastic deposits of biogenic origin (i.e.,

541 marine bioproductite see [Lucas and Prevôt-Lucas, 1995](#)). The continental influence is
542 marked there only by occasional rare terrestrial fossils in the phosphate levels. The
543 terrestrial sediment input in the Moroccan phosphate basins was low, due maybe to the flat
544 topography in the hinterland (low hydrodynamism and erosion) and perhaps also to the
545 filtering role of coastal mangroves (e.g., [Fechner, 1988](#)). However, the river water and/or
546 sub-terrain water draining from the hinterland towards the basin may have had some
547 effects, at least in the transportation of the floating bodies/carcasses of the Ouled Abdoun
548 mammals ([Gheerbrant et al., 2003](#)).

549 The REE element patterns, however, were still compatible with oxic seawater ([Figure 4](#)).
550 Though the Ce/Ce* ratios are somewhat higher here than in the younger samples ([Figure 5](#)),
551 the stratigraphic changes in these values were interpreted as a reflection of the enhanced
552 opening of the Atlantic Ocean and hence a better connection with the global oceanic
553 circulation ([Kocsis et al., 2016](#)). In this sense the $^{87}\text{Sr}/^{86}\text{Sr}$ data of the Cretaceous and older
554 Paleocene samples could indicate somewhat more restricted conditions in which seawater
555 was slightly locally controlled. First-order sea-level changes during the late Cretaceous and
556 early Paleogene indicate global regression (e.g., [Hardenbol et al., 1998](#); [Snedden and Liu,](#)
557 [2010](#); [van der Meer et al., 2017](#)), which could support the semi-confined situation in the
558 Moroccan phosphate basins. Interestingly, the $^{87}\text{Sr}/^{86}\text{Sr}$ data reported from foraminifera
559 from the South Atlantic (Walvis Ridge) also yielded rather higher ratios than the global
560 ocean Sr-isotope curve during this part of the Paleocene ([Hodell et al., 2007](#)). Even if some
561 samples were clearly affected by diagenesis the lowest Sr-isotopic ratios have a perfect fit
562 with McArthur's curve between 52 and 58 Ma ([Figure 7b](#)), but the older samples are above
563 the curve at the Walvis Ridge as well. This might hint at a common cause altering the Sr-
564 budget and its mixing in the Central and South Atlantic, which may have been related to the
565 formation of wider scales of global oceanic circulation. Nevertheless, better suited samples
566 covering larger regions are needed to seriously assess this scenario.

567

568 *5.4. Mammal ecology based on stable isotope chemistry*

569 The oxygen and carbon isotopic compositions of fossil mammal teeth are often used for
570 palaeoecological and palaeoenvironmental reconstructions (e.g., [Ayliffe et al., 1994](#); [Kohn](#)
571 [and Cerling, 2002](#); [Amiot et al., 2004](#)), even for extinct taxa of the Paleocene and Eocene for
572 which the physiology of the animals is more difficult to assess (e.g., [Liu et al., 2008](#); [Secord](#)

573 et al., 2008; Kocsis et al., 2014b; Mahboubi et al., 2014; Tütken, 2014). Nevertheless, based
574 on the tooth morphology the mammals from the Ouled Abdoun Basin investigated here
575 were all herbivores (Ypresian proboscideans are especially folivorous specialists). Their body
576 fluid $\delta^{18}\text{O}$ depends on the ingested water, which mainly came from drinking sources and/or
577 dietary plant water, while their $\delta^{13}\text{C}$ was entirely driven by their diet and can be related to
578 the palaeoflora (e.g., Kohn and Cerling, 2002). The growth of teeth and bones record these
579 ecological parameters, and can be used to gain information about the past environment.
580 The teeth and bones are composed of bioapatite with a simplified formula of $\text{Ca}_5(\text{PO}_4,$
581 $\text{CO}_3)_3(\text{OH}, \text{CO}_3)$. From the oxygen bearing ions, the phosphate ion dominates the apatite
582 structure and is considered to be the most resistant to diagenesis due to the strong P-O
583 bond. Therefore, the phosphate oxygen isotopic composition ($\delta^{18}\text{O}_{\text{PO}_4}$) can provide the most
584 reliable ecological information. To further evaluate possible alterations, enamel, dentin and
585 bone can be analyzed separately and compared, with the enamel considered to be less
586 prone to diagenetic alteration (e.g., Zazzo et al., 2004). The $\delta^{18}\text{O}_{\text{PO}_4}$ data from the Moroccan
587 mammals do not show consistent variations across these materials, but the $\delta^{13}\text{C}$ of *O.*
588 *grandis* and *P. escuilliei* clearly point towards higher values in the less dense material of
589 bone and dentine (Figure 8). This can be interpreted as meaning that the $\delta^{18}\text{O}_{\text{PO}_4}$ data are
590 more robust across the various materials; however the isotope values from the structural
591 carbonate underwent partial interaction and exchange with the marine pore fluid in the
592 depositional environment. For this reason, only the enamel data are taken into account
593 when the ecology of these ancient mammals is discussed, even for the $\delta^{18}\text{O}_{\text{PO}_4}$ results.

594 The overall average $\delta^{18}\text{O}_{\text{PO}_4}$ value for the enamel is $20.0 \pm 1.3 \text{‰}$ ($n = 12$), and no obvious
595 species-specific variations occur. The largest variation is between two specimens of
596 *Daouitherium rebouli* (MNHN.F PM3 and PM65), with a nearly 3 ‰ difference in their
597 enamel values (Figure 8). The relationship between mammal $\delta^{18}\text{O}_{\text{PO}_4}$ and the local meteoric
598 water (i.e., consumed water) can be taxon specific and dependent also on the relative
599 humidity (e.g., Kohn, 1996; Ayliffe et al., 1994; Kohn and Cerling, 2002). This can be
600 complicated further by the migration of animals, seasonal variations, and/or locally available
601 water sources that are different from the local meteoric water. Moreover, the physiology of
602 the investigated taxa is hard to assess, and for these reasons Amiot et al. (2004)'s globally
603 compiled mammal database and latitude adjusted $\delta^{18}\text{O}_{\text{PO}_4}$ versus meteoric water correlation

604 is used here, with the assumption that the ancient mammals' body fluids were affected by
605 the local meteoric fluid (i.e., drinking water or plant water). This would yield an average of -
606 4.2 ± 1.3 ‰ (n = 12) local meteoric water isotopic composition, which in turn can be linked
607 to a mean annual temperature of 20.4 ± 3.0 °C (n = 12) (see [Amiot et al., 2004](#)) for the late
608 Paleocene and early Eocene ([Figure 8](#)). This is about 2-3 °C degrees higher than today's MAT
609 for the coastal area of Morocco (e.g., Agadir-Casablanca, see [climate-data.org](#)). Considering
610 the palaeolatitudinal temperature gradient for a greenhouse climate regime ([Amiot et al.,](#)
611 [2004](#)) and the fact that the studied sites were not much further south (~22°-24°N, see [van](#)
612 [Hinsbergen et al., 2015](#)) than today, the absolute MAT result we obtained seems
613 reasonable. Nevertheless, the higher isotopic composition in the bioapatite indicates a
614 higher isotopic composition in the ingested water, which in turn reflects a higher MAT
615 ([Figure 8](#)). The high $\delta^{18}\text{O}_{\text{PO}_4}$ values for one of the *D. rebouli* (MNHN.F PM3) and Hyracoidea
616 (MNHN.F PM52) teeth may reflect the effects of the Early Eocene Climatic Optimum (EECO),
617 with a related global temperature rise and/or enhanced dryer periods (i.e., more
618 evaporation of the drinking sources). However, only a few samples were analyzed and the
619 high $\delta^{18}\text{O}_{\text{PO}_4}$ values and related temperature calculations might be biased by the migration
620 of the animals or strong evaporation of the local drinking source. Geochemical analysis of
621 the sediments and the marine fossils had also detected the EECO event in the phosphorite
622 series ([Yans et al., 2014](#); [Kocsis et al., 2014](#)). Moreover, the stratigraphic average MATs
623 reveals a rise of about 5 °C degree from the early Ypresian to mid-Ypresian ([Figure 8](#)), which
624 agrees well with the peak of the EECO and related ΔMAT estimates (e.g., [Hyland et al.](#)
625 [2016](#)). If these analyses indeed reflect the EECO, then the proposed stratigraphic origin of
626 these taxa (*D. rebouli* & Hyracoidea) in Horizons 3 (upper part) and 2 is further confirmed
627 (see section 4.2 and [Figure 6](#)).

628 The average enamel $\delta^{13}\text{C}$ value is -7.9 ± 0.8 ‰ (n = 5), which can be translated to a
629 consumed plant isotopic composition of -22 ± 0.8 ‰ (e.g., [Kohn and Cerling, 2002](#); [Figure 8](#)).
630 This mean value is at the very high end of a C3 palaeoflora, and because the C4
631 photosynthetic pathway was not yet widespread (i.e., high $\delta^{13}\text{C}_{\text{plant}}$), this suggests a very dry
632 Thanetian-middle Ypresian local continental palaeoecosystem with mean annual
633 precipitation well below 500 mm ([Kohn, 2010](#)). A dry arid early Eocene climate was also
634 suggested by palynology and palaeobotanic finds in the Moroccan south Atlas, which

635 indicated mangrove and marsh vegetation along the palaeo-coast, together with a fairly dry
636 and scarcely vegetated hinterland (Mohr, 1986; Mohr and Fehner, 1986; Fehner, 1988).
637 Mangrove vegetation along the coast line is also predicted by models (Descombes et al.,
638 2018; Couvreur et al., 2021). The presence of early diagenetic dolomite and gypsum in some
639 of these deposits were also interpreted as a consequence of an arid climate during the
640 Ypresian, and only a low amount of seasonal precipitation was proposed (e.g., Mohr, 1986;
641 Fehner, 1988). In addition, the rarity of detritic (clastic) material in the phosphate basins
642 (Lucas and Prevôt-Lucas, 1995), and the high quantity of palygorskite clay mineral in the
643 Paleogene deposits in the Atlas (Daoudi, 2004; Knidiri et al., 2014) and offshore Morocco
644 (e.g., Chamley et al., 1980), would further suggest a dry semi-arid late Paleocene - Ypresian
645 climate in the region. By contrast, Herbig and Gregor (1990) have advocated a tropical
646 humid climate based on the discovery of mangrove macro-plant remains of *Nypa* palms
647 from Thanetian-Ypresian levels in the Ouarzazate Basin, based on a re-evaluation of early
648 available data.

649 In the view of the mammal enamel $\delta^{13}\text{C}$ values from the Ouled Abdoun Basin, the
650 ingested plants must have lived in water-stressed, and maybe also salinity-stressed (i.e.,
651 mangrove vegetation, e.g., Wei et al., 2008) environment, supporting the hypothesis of arid
652 late Paleocene - Ypresian climatic conditions in the region. The minimal variation in the $\delta^{13}\text{C}$
653 values through time could reflect a steady dry ecosystem along the Moroccan coastline
654 during the Paleocene-Eocene. Still, the EECO warm period may have stressed the
655 palaeoflora further, and even somewhat higher values of $\delta^{13}\text{C}$ may be expected (e.g., even
656 more water stress, Farquhar et al., 1989). However, this may have been compensated by a
657 higher relative humidity and / or higher atmospheric pCO_2 during the EECO (Pearson and
658 Palmer, 2000; Schubert and Jahren, 2002). The EECO warming is likely also to have driven an
659 evolution to increased size the Ouled Abdoun mammals (e.g., Yans et al., 2014). The
660 embrithopods lineage *S. minor*- *S. major* (Gheerbrant et al., 2020) records a significant
661 increase in size during the early-middle Ypresian. Similar size changes are observed between
662 *Phosphatherium* and *Daouitherium*, however with much less stratigraphic difference
663 between these taxa as inferred here (Figure 6).

664

665 6. Conclusions

666 The rare but diverse terrestrial mammal fossils from the Ouled Abdoun phosphorite are
667 proven to have a similar diagenetic history to that of the marine fossils. This is reflected by a
668 similar REE distribution and stratigraphy matched Ce/Ce* and Pr/Pr* ratios. The Ce/Ce*
669 variation along the phosphate series either confirmed previous known origins or helped to
670 estimate the stratigraphic provenance of the Ouled Abdoun mammal specimens whose
671 origin was unknown. Exchanges with marine pore fluid affected the enamel, dentine, and
672 bone differently, with the enamel being the most robust to alteration, and hence the best to
673 use for investigation of the palaeoenvironment of the African Paleogene mammals from the
674 Ouled Abdoun sites.

675 This study has identified ten chemostratigraphic horizons in the Maastrichtian-Ypresian
676 phosphates series of the Ouled Abdoun Basin. It confirms most of the previously proposed
677 age determinations for the mammals found in the Ouled Abdoun Basin, but with some
678 corrections and additions. One new conclusion is that all the Paleocene mammal material
679 studied here ranges from the Selandian to the lower Thanetian (uppermost Bed IIb to the
680 base of Bed IIa). In particular, *O. grandis* does not come from the upper part of Bed IIa (late
681 Thanetian) but is actually a coexisting lineage with *O. daouiensis*, which highlights the little-
682 known radiation of the stem paenungulates. The study suggests that some mammal species
683 might have a wider stratigraphical extension than previously known, including across the
684 PETM. However, as the Ouled Abdoun mammal material remains scarce, it is unknown if
685 this relates to the presence of undetermined chronospecies or to the succession of
686 intraspecific diachronic populations. Chemostratigraphic results indicate that the
687 embrithopod *S. major* likely comes from the uppermost phosphates levels (late Middle
688 Ypresian) of the Ouled Abdoun series, and is the youngest Paleogene mammal known in the
689 Ouled Abdoun Basin.

690 While the mammal enamel yielded the highest $^{87}\text{Sr}/^{86}\text{Sr}$ ratios, indicating the composition
691 of the hinterland rocks (a terrestrial Sr-source), the ratios for the shark tooth enameloid
692 from the latest Paleocene to early Eocene are compatible with the open ocean Sr isotope
693 ratios of the time. Older marine fossils deviate from the global Sr-isotope curve, which most
694 probably reflects alteration or may link to somewhat restricted conditions and a variable Sr-
695 budget in the African coastal basins of the Atlantic Ocean. The enamel derived oxygen and
696 carbon isotopic compositions of the Ouled Abdoun mammal teeth point to warm and arid
697 climatic conditions along the Atlantic palaeocoast of North Western Africa. In addition, an

698 increase about 5 °C degrees in MAT was recorded by the mid-Ypresian, which is linked to
699 the EECO. Our geochemical study of the Ouled Abdoun fossils provides support for the
700 evolution of endemic African lineages of placental mammals, such as the early embriothopod
701 *Stylolophus*, during the EECO event.

702

703 **Acknowledgements**

704 The research was conducted under L.K.'s Ambizione research grants (Nr. PZ00P2_126407 &
705 PZ00P2_145115/1 – Switzerland), but in the later phase of the project LK also received
706 support from his URC Grant from Universiti Brunei Darussalam (UBD/PNC2/2/RG/1(325)).
707 The help from both funding agencies is much appreciated. This study benefited from the
708 paleontological “Phosphapal” collaborative Agreement with the Ministère de l'Energie, des
709 Mines, de l'Eau et de l'Environnement (MEMEE), the Office Chérifien des Phosphates (OCP
710 SA) of Morocco, the Muséum National d'Histoire Naturelle (MNHN, Paris), and the
711 Universities Cadi Ayyad (Marrakech, Morocco) and Chouaib Doukkali (El Jadida, Morocco).
712 We are most grateful to the Geological Survey of the OCP mining centre of Khouribga for
713 help with the field work. Identification of the matrix related selachian fauna by Prof. Henri
714 Cappetta (CNRS, Université de Montpellier II, France) is much appreciated. Constructive
715 comments on a previous version of the manuscript by the editor Thomas Algeo, and three
716 reviewers, Živilė Žigaitė and 2 anonymous ones, are much appreciated. We thank Malcolm
717 R. Anderson for proofreading the updated manuscript.

718

719 **References**

- 720 Akhtar, A.A., Santi, M.L., Griffiths, L.M., Becker, M., Eagle, A.R., Kim, S., Kocsis, L., Rosenthal, Y., Higgins, J.A.,
721 2020. A record of the $\delta^{44}/^{40}\text{Ca}$ and [Sr] of seawater over the last 100 million years from fossil
722 elasmobranch tooth enamel. *Earth and Planetary Science Letters* 543,
723 doi.org/10.1016/j.epsl.2020.116354.
- 724 Amiot, R., Lecuyer, C., Buffetaut, E., Fluteau, F., Legendre, S., Martineau, F., 2004. Latitudinal temperature
725 gradient during the Cretaceous Upper Campanian Middle Maastrichtian: $\delta^{18}\text{O}$ record of continental
726 vertebrates. *Earth Planet. Sci. Lett.* 226, 255–272. <http://dx.doi.org/10.1016/j.epsl.2004.07.015>.
- 727 Arambourg, C., 1952. Les vertébrés fossiles des gisements de phosphates (Maroc-Algérie-Tunisie). *Notes*
728 *Mémoires du Service géologique du Maroc* 92, pp. 1–372.
- 729 Arppe L., Karhu J.A., Vartanyan S.L., 2009. Bioapatite $^{87}\text{Sr}/^{86}\text{Sr}$ of the last woolly mammoths – implications for
730 the isolation of Wrangel Island. *Geology* 37, 347–350.
- 731 Ayliffe, L.K., Chivas, A.R., Leakey, M.G., 1994. The retention of primary oxygen isotope compositions of fossil
732 elephant skeletal phosphate. *Geochim. Cosmochim. Acta* 58, 5291–5298.
733 [http://dx.doi.org/10.1016/0016-7037\(94\)90312-3](http://dx.doi.org/10.1016/0016-7037(94)90312-3).
- 734 Bardet, N., Gheerbrant, E., Noubhani, A., Cappetta, H., Jouve, S., Bourdon, E., Pereda Suberbiola, X., Jalil, N.-E.,
735 Vincent, P., Houssaye, A., Solé, F., El Houssaini, Kh., Adnet, S., Rage, J.-C., Lapparent de Broin, F., Sudre,
736 J., Bouya, B., Amaghazaz, M., Meslouh, S., 2017. Les vertébrés fossiles des phosphates crétacés-

737 paléogènes (72,1-47,8 Ma) du Maroc, in Zouhri, S. ed., Paléontologie des Vertébrés du Maroc: état des
738 connaissances. Mémoire de la Société Géologique de France, v. 180, p. 351–452.

739 Bau, M., Dulski, P., 1996. Distribution of yttrium and rare-earth elements in the Penge and Kuruman iron-
740 formations, Transvaal Supergroup, South Africa. *Precambrian Res.* 79, 37–55.

741 Blum, J.D., Talianferro, E.H., Weisse, M.T., Holmes, R.T., 2000. Changes in Sr/Ca, Ba/Ca and 87Sr/86Sr ratios
742 between two forest ecosystems in the northeastern USA. *Biogeochemistry* 49, 87–101.

743 Botfalvai, G., Csiki-Sava, Z., Kocsis, L., Gáspár, A., Magyar, J., Bodor, R.E., Ţabără, D., Ulyanov, A., Makádi, L.,
744 2021. X' marks the spot! Sedimentological, geochemical and palaeontological investigations of Late
745 Cretaceous (Maastrichtian) vertebrate fossil localities from Vălioara Valley (Densus-Ciula Formation,
746 Hateg Basin, Romania). *Cretaceous Research*, 123.

747 Bourdon, E., Bouya, B., Iarochene, M. 2005. Earliest African neornithine bird: A new species of
748 Prophaethontidae (Aves) from the Paleocene of Morocco. *Journal of Vertebrate Paleontology*, 25 (1),
749 157–170.

750 Bruland, K.W., Lohan, M.C., 2003. Controls of Trace Metals in Seawater. In: Holland, H.D., Turekian, K.K. (eds)
751 *Treatise on Geochemistry*, vol. 6. pp 23–47.

752 Cappetta, H., Bardet, N., Pereda-Suberbiola, X., Adnet, S., Akkrim, D., Amalik, M., Benabdallah, A., 2014.
753 Marine vertebrate faunas from the Maastrichtian phosphate deposits of the Benguérir area (Ganntour
754 Basin, Morocco): biostratigraphy, palaeobiogeography and palaeoecology. *Palaeogeogr. Palaeoclimatol.*
755 *Palaeoecol.* 409, 217–238.

756 climate-data.org

757 Chamley H., Giroud d'Argoud G., Robert C., 1980. Clay mineralogy of Cretaceous and Cenozoic sediments off
758 the Moroccan margin, Deep Sea Drilling Project sites 415, 416. Initial Rep. Deep Sea Drilling Proj., 50,
759 715–721.

760 Cosmidis, J., Benzerara, K., Menguy, N., Arning, E., 2013. Microscopy evidence of bacterial microfossils in
761 phosphorite crusts of the Peruvian shelf: Implications for phosphogenesis mechanisms. *Chemical*
762 *Geology*, 359, 10–22.

763 Couvreur, T.L.P., Dauby, G., Blach-Overgaard, A., Deblauwe, V., Dessein, S., Droissart, V., Hardy, O.J., Harris,
764 D.J., Janssens, S.B., Ley, A.C., Mackinder, B.A., Sonké, B., Sosef, M.S.M., Stévant, T., Svenning, J.-C.,
765 Wieringa, J.J., Faye, A., Missoup, A.D., Tolley, K.A., Nicolas, V., Ntie, S., Fluteau, F., Robin, C.,
766 Guillocheau, F., Barboni, D., Sepulchre, P., 2021. Tectonics, climate and the diversification of the
767 tropical African terrestrial flora and fauna. *Biol. Rev.* 96, 16–51.

768 Daoudi L., 2004. Palygorskite in the uppermost Cretaceous-Eocene Rocks from Marrakech High Atlas, Morocco.
769 *Journal of African Earth Sciences*, 39, 353–358.

770 Descombes, P., Gaboriau, T., Albouy, C., Heine, C., Leprieur, F., Pellissier, L., 2018. Linking species
771 diversification to palaeo-environmental changes: a processbased modelling approach. *Global Ecology*
772 *and Biogeography* 27, 233–244.

773 Domingo, L., Cuevas-González, J., Grimes, S.T., Hernández Fernández, M., López-Martínez, N., 2009. Multiproxy
774 reconstruction of the paleoclimate and paleoenvironment of the Middle Miocene Somosaguas site
775 (Madrid, Spain) using herbivore tooth enamel. *Palaeogeogr. Palaeoclimatol. Palaeoecol.*, 272, 53–68.

776 El Assel, N., Kchikach, A., Durllet, C., AlFedy, N., El Hariri, K., Charroud, M., Jaffal, M., Jourani, E., Amaghaz, M.,
777 2013. Mise en évidence d'un Sénonien gypseux sous la série phosphatée du bassin des Ouled Abdoun:
778 Un nouveau point de départ pour l'origine des zones dérangées dans les mines à ciel ouvert de
779 Khouribga, Maroc. *Estudios Geológicos*, 69(1), 47–70. <https://doi.org/10.3989/egeol.40781.168>

780 Elderfield, H., Pagett, R., 1986. Rare earth elements in ichthyoliths: variations with redox conditions and
781 depositional environment. *Sci. Total Environ.* 49, 175–197.

782 El Haddi, H., 2014. Les silicifications de la série phosphatée des Ouled Abdoun (Maastrichtien-Lutétien Maroc):
783 Sédimentologie, Minéralogie, Géochimie et Contexte Génétique, [PhD Thesis]: Université Hassan II de
784 Casablanca, Faculté des Sciences Ben M'Sik, 135 p.

785 Farquhar G.D., Ehleringer J.R., Hubick, K.T., 1989. Carbon isotope discrimination and photosynthesis. *Ann. Rev.*
786 *Plant Physiol. Plant Mol. Biol.* 40, 503–537.

787 Fechner, G.G., 1988. Selected palynomorphs from the Lower to Middle Eocene of the south Atlas Border Zone
788 (Morocco) and their environmental significance. *Palaeogeogr. Palaeoclimatol. Palaeoecol.* 65, 73–79.

789 Gaillardet, J., Viers, J., Dupré, B., 2003. Trace Elements in River Waters. In: Holland, H.D., Turekian, K.K. (eds)
790 *Treatise on Geochemistry*, vol. 5. Pp. 225–272.

791 Gheerbrant, E., 2009. Paleocene emergence of elephant relatives and the rapid radiation of African ungulates.
792 *Proceedings of the National Academy of Sciences* 106, 10717–10721.

793 Gheerbrant, E., Sudre, J., Cappetta, H., Bignot, G., 1998. *Phosphatherium escuilliei* du Thanétien du bassin des
794 Ouled Abdoun (Maroc), plus ancien proboscidiien (Mammalia) d'Afrique. *Geobios* 30, 247–269.

795 Gheerbrant, E., Sudre, J., Iarochene, M., Moumni, A., 2001. First ascertained African "condylarth" mammals
796 (primitive ungulates : cf. *Bulbulodontata* & cf. *Phenacodonta*) from the Earliest Ypresian of the Ouled
797 Abdoun Basin, Morocco. *Journal of Vertebrate Paleontology* 21, 107–118.

798 Gheerbrant, E., Sudre, J., Cappetta, H., Iarochène, M., Amaghaz, M., Bouya, B., 2002. A new large mammal
799 from the Ypresian of Morocco: Evidence of surprising diversity of early proboscideans. *Acta*
800 *Palaeontologica Polonica*. 47 (3), 493–506.

801 Gheerbrant, E., Sudre, J., Cappetta, H., Mourer-Chauvire, C., Bourdon, E., Iarochene, M., Amaghaz, M., Bouya,
802 B., 2003. Les localités à mammifères des carrières de Grand Daoui, Bassin des Ouled Abdoun, Maroc,
803 Yprésien : premier état des lieux. *Bulletin de la Société Géologique de France* 174, 279–293.

804 Gheerbrant, E., Sudre, J., Tassy, P., Amaghaz, M., Bouya, B., Iarochène, M., 2005. "Nouvelles données sur
805 *Phosphatherium escuilliei* (Mammalia, Proboscidea) de l'Eocene inférieur du Maroc, apports à la
806 phylogeny of the Proboscidea et the ongulés lophodontes". *Geodiversitas*. 27 (2), 239–333.

807 Gheerbrant, E., Bouya, B., Amaghaz, M., 2012. Dental and cranial anatomy of *Eritherium azzouorum* from the
808 Paleocene of Morocco, earliest known proboscidean mammal. *Palaeontographica, A* 297, 151–183.

809 Gheerbrant, E., Amaghaz, M., Bouya, B., Goussard, F., Letenneur, C., 2014. *Ocepeia* (middle Paleocene of
810 Morocco): the oldest skull of an afrotherian mammal. *PLOS One* 9, 1–30 (DOI:
811 10.1371/journal.pone.0089739).

812 Gheerbrant, E., Cappetta, H., Lapparent de Broin, F. de, Rage, J.-C., and Tabuce, R., 2017. Les faunes de
813 vertébrés marins et terrestres du Paléogène du Bassin d'Ouarzazate, Maroc, in Zouhri, S. ed.,
814 Paléontologie des Vertébrés du Maroc: état des connaissances. Mémoire de la Société Géologique de
815 France, v. 180, p. 485–525.

816 Gheerbrant, E., Schmitt, A., Kocsis, L., 2018. Early African fossils elucidate the origin of embrithopod mammals.
817 – *Current Biology* 28, 1–7. – <https://doi.org/10.1016/j.cub.2018.05.032>

818 Gheerbrant, E., Khaldoune, F., Schmitt, A., Tabuce, R., 2020. Earliest embrithopod mammals (Afrotheria,
819 Tethytheria) from the Early Eocene of Morocco: anatomy, systematics and phylogenetic significance.
820 *Journal of Mammal Evolution*. <https://doi.org/10.1007/s10914-020-09509-6>

821 Goettig, P., Magdolen, V., Brandstetter, H., 2010. Natural and synthetic inhibitors of kallikrein-related
822 peptidases (KLKs). *Biochimie* 92, 1546–1567.

823 Hardenbol, J., Thierry, J., Farley, M.B., Jacquin, T., de Graciansky, P.-C., Vail, P.R., 1998. Mesozoic and Cenozoic
824 sequence stratigraphy of European basins. *SEPM Spec. Publ.* 60, 3–13.

825 Harrell, T.L., Pérez-Huerta, A., Phillips, G., 2016. Strontium isotope age-dating of fossil shark tooth enameloid
826 from the Upper Cretaceous Strata of Alabama and Mississippi, USA. *Cretac. Res.* 62, 1–12.

827 Herbig, H.G., Gregor H.J., 1990. The mangrove-forming palm *Nypa* from the early Paleogene of southern
828 Morocco. *Paleoenvironment and paleoclimate*. In: *Géologie Méditerranéenne*. Tome 17, numéro 2,
829 1990. pp. 123–137.

830 Herwartz, D., Tütken, T., Münker, C., Jochum, K.P., Stoll, B., Sander, P.M., 2011. Timescales and mechanisms of
831 REE and Hf uptake in fossil bones. *Geochim. Cosmochim. Acta* 75, 82–105.

832 Herwartz, D., Tütken, T., Jochum, K.P., Sander, P.M., 2013. Rare earth element systematics of fossil bone
833 revealed by LA-ICPMS analysis. *Geochim. Cosmochim. Acta* 103, 161–183.

834 Hodell, D.A., Kamenov, G.D., Hathorne, E.C., Zachos, J.C., Röhl, U., Westerhold, T., 2007. Variations in the
835 strontium isotope composition of seawater during the Paleocene and early Eocene from ODP Leg 208
836 (Walvis Ridge). *Geochem Geophys Geosyst* 8:Q09001. doi:10.1029/2007GC001607

837 Hoppe, K.A., Koch, P.L., Carlson, R.W., Webb, S.D., 1999. Tracking mammoths and mastodons: reconstruction
838 of migratory behavior using strontium isotope ratios. *Geology* 27, 439–442.

839 Hyland, G.E., Sheldon, D.N., Cotton, M.J. 2017. Constraining the early Eocene climatic optimum: A terrestrial
840 interhemispheric comparison. *GSA Bulletin*, 129 (1-2), 244–252.

841 Ingram, B.L., 1995. High-resolution dating of deep-sea clays using Sr isotopes in fossil fish teeth. *Earth and*
842 *Planetary Science Letters* 134, 545–555.

843 Knidiri, A., Daoudi, L., El Ouahabi, M., Rhouta, B., Rocha, F., Fagel, N., 2014. Palaeogeographic controls on
844 palygorskite occurrence in Maastrichtian-Palaeogene sediments of the western High Atlas and Meseta
845 Basins (Morocco). *Clay Minerals* 49, 595–608.

846 Kocsis, L., Vennemann, T.W., Fontignie, D., 2007. Migration of sharks into freshwater systems during the
847 Miocene and implications for Alpine paleoelevation. *Geology*, 35, 451–454.

848 Kocsis, L., Osi, A., Vennemann, T.W., Trueman, N.C., Palmer, R.M., 2009. Geochemical study of vertebrate
849 fossils from the Upper Cretaceous (Santonian) Csehbánya formation (Hungary): evidence for a

850 freshwater habitat of mosasaurs and pycnodont fish. *Palaeogeogr. Palaeoclimatol. Palaeoecol.* 280,
851 532–542.

852 Kocsis, L., Trueman, C.N., Palmer, M., 2010. Protracted diagenetic alteration of REE contents in fossil
853 bioapatites: direct evidence from Lu–Hf isotope systematics. *Geochim. Cosmochim. Acta* 74, 6077–
854 6092.

855 Kocsis, L., Ounis, A., Chaabani F., Salah, N.M., 2013. Paleoenvironmental conditions and strontium isotope
856 stratigraphy in the Paleogene Gafsa Basin (Tunisia) deduced from geochemical analyses of phosphatic
857 fossils. *International Journal of Earth Sciences* 102, 1111–1129.

858 Kocsis, L., Gheerbrant, E., Mouflih, M., Cappetta, H., Yans, J., Amaghaz, M., 2014a. Comprehensive stable
859 isotope investigation of marine biogenic apatite from the late Cretaceous-early Eocene phosphate beds
860 of Morocco. – *Palaeogeography, Palaeoclimatology, Palaeoecology*, 394, 74–88.

861 Kocsis, L., Ozsvart, P., Becker, D., Ziegler, R., Scherler, L., Codrea, V., 2014b. Orogeny forced terrestrial climate
862 variation during the late Eocene-early Oligocene in Europe. *Geology* 42, 727–730.
863 <http://dx.doi.org/10.1130/g35673.1>.

864 Kocsis, L., Vennemann, T., Ulianov, A., Brunnschweiler, J.M., 2015. Tracing bull shark (*Carcharhinus leucas*)
865 freshwater habitats in Fiji by chemical and isotopic compositions of their teeth. *Environ. Biol. Fish* 98
866 (6), 1609–1622.

867 Kocsis, L., Gheerbrant, E., Mouflih, M., Cappetta, H., Ulianov, A., Chiaradia, M., Bardet, N., 2016. Gradual
868 changes in upwelled seawater conditions (redox, pH) from the late Cretaceous through early Paleogene
869 at the northwest coast of Africa: Negative Ce anomaly trend recorded in fossil bio-apatite. *Chemical*
870 *Geology* 421, 44–54.

871 Kohn, M.J., 1996. Predicting animal $\delta O-18$: Accounting for diet and physiological adaptation. *Geochim.*
872 *Cosmochim. Acta* 60, 4811–4829. [http://dx.doi.org/10.1016/s0016-7037\(96\)00240-2](http://dx.doi.org/10.1016/s0016-7037(96)00240-2).

873 Kohn, M.J., 2010. Carbon isotope compositions of terrestrial C3 plants as indicators of (paleo) ecology and
874 (paleo)climate. *National Academy of Sciences Proceedings*, v. 107, p. 19691–19695,
875 doi:10.1073/pnas.1004933107.

876 Kohn, M.J., Cerling, T.E., 2002, Stable isotopes of biological apatite, in Kohn, M.L., et al., eds., *Phosphates:*
877 *Geochemical, geobiological and materials importance: Mineralogical Society of America Reviews in*
878 *Mineralogy Volume 48*, p. 455–488.

879 Kowal-Linka, M., Jochum, K.P., Surmik, D., 2014. LA-ICP-MS analysis of rare earth elements in marine reptile
880 bones from the Middle Triassic bonebed (Upper Silesia, S Poland): impact of long-lasting diagenesis, and
881 factors controlling the uptake. *Chem. Geol.* 363, 213–228.

882 Lécuyer, C., Reynard, B., Grandjean, P., 2004. Rare earth element evolution of Phanerozoic seawater recorded
883 in biogenic apatites. *Chem. Geol.* 204, 63–102.

884 Liu, A.G.S.C., Seiffert, E.R., Simons, E.L., 2008. Stable isotope evidence for an amphibious phase in early
885 proboscidean evolution. *Proceedings of the National Academy of Sciences* 105, 5786–5791.
886 <https://doi.org/10.1073/pnas.0800884105>

887 Lucas, J., Prevôt-Lucas, L., 1995. Tethyan phosphates and bioproductites. In: Nairn, A.E. (Ed.), *The Ocean Basins*
888 *and Margins. The Tethys Ocean*, vol. 8. Plenum Press, pp. 367–391.

889 Mahboubi, S., Bocherens, H., Scheffler, M., Benammi, M., Jaeger, J.-J., 2014. Was the Early Eocene
890 proboscidean *Numidotherium koholense* semi-aquatic or terrestrial? Evidence from stable isotopes and
891 bone histology. *Comptes Rendus Palevol* 13, 501–509. <https://doi.org/10.1016/j.crpv.2014.01.002>

892 McArthur, J.M., Howarth, R.J., Shields, G.A., Zhou, Y. 2020. Strontium isotope stratigraphy, Chapter 7. In:
893 Gradstein, F.M., Ogg, J.G., Schmitz, M.D., Ogg, G.M. (Eds.), *A Geologic Time Scale*, Elsevier B.V., Vol 1 of
894 2, pp. 211–238.

895 MacFadden, B.J., Labs-Hochstein, J., Hulbert Jr., R.C., Baskin, J.A., 2007. Revised age of the late Neogene terror
896 bird (*Titanis*) in North America during the Great American interchange. *Geology* 35, 123–126.

897 McLennan, S.M. 1989. Rare earth elements in sedimentary rocks: Influence of provenance and sedimentary
898 processes. In: Lipin RB, McKay AG (Eds.), *Geochemistry and Mineralogy of Rare Earth Elements. Review*
899 *in Mineralogy and Geochemistry* vol. 21, pp. 169–200.

900 Metzger, C.A., Terry, D.O., Grandstaff, D.E., 2004. Effect of paleosol formation on rare earth element
901 signatures in fossil bone. *Geology* 32, 467–500.

902 Mohr, B., 1986. Palynologischer Nachweis eines Mangrovenbiotops in der Südatlas-Randzone (Marokko) und
903 seine paläoökologische Bedeutung. *Documenta naturae* 33, 20–28.

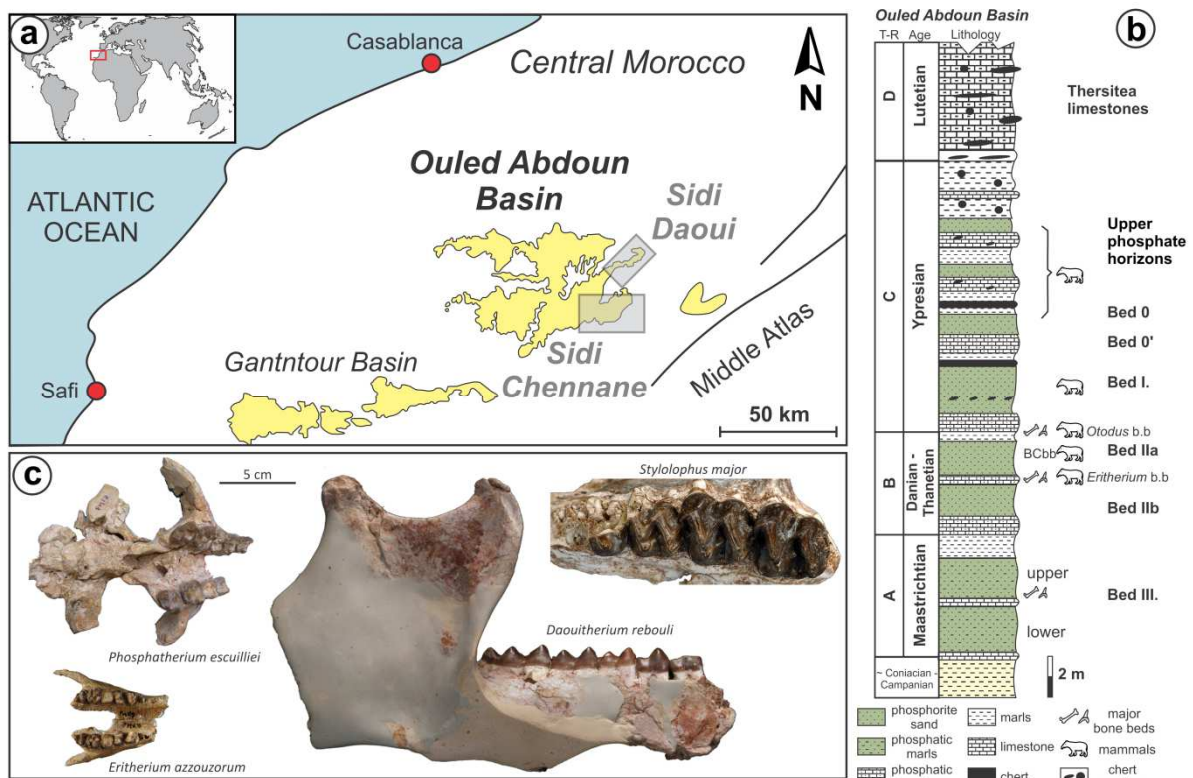
904 Mohr, B., Fechner, G., 1986. Eine eozäne Mikroflora (Sporomorphae und Dinoflagellaten-Zysten) aus der
905 Südatlas-Randzone westlich Boumalne du Dadès (Marokko). *Berl. Geowiss. Abh. A.* 66, 414–481.

- 906 Mouflih, M., 2015. Les phosphates du Maroc central et du Moyen Atlas (Maastrichtien-Lutétien, Maroc):
907 Sédimentologie, stratigraphie séquentielle, contexte génétique et valorisation. Doctorat d'Etat Es-
908 sciences. Université Cadi Ayyad de Marrakech, Maroc 246 p.
- 909 Noubhani, A., Cappetta, H., 1997. Les Orectolobiformes, Carcharhiniformes et Myliobatiformes
910 (Elasmobranchii, Neoselachii) des bassins à phosphate du Maroc (Maastrichtien-Lutétien basal).
911 Systématique, biostratigraphie, évolution et dynamique des faunes. *Palaeo-Ichthyologica* 8, 1–327.
- 912 Office Chérifien des Phosphates, 1989. The phosphates basins of Morocco. In: Notholt, A.J.G., Sheldon, R.P.,
913 Davidson, D.F. (Eds.), *Phosphates Deposits of the World, Phosphate Rock Resources*. Cambridge
914 University Press, Cambridge, pp. 301–311.
- 915 Ollivier-Pierre, M.F., 1982. La microflore du Paléocène et de l'Eocène des séries phosphatées des gantour
916 (Maroc). *Sci. Géol. Bull.* 35 (3), 117–127.
- 917 Pearce, N.J.G., Perkins, W.T., Westgate, J.A., Gorton, M.P., Jackson, S.E., Neal, C.R., Chenery, S.P., 1997. A
918 compilation of new and published major and trace element data for NIST SRM 610 and NIST SRM 612
919 glass reference materials. *Geostand. Geoanal. Res.* 21, 115–144.
- 920 Pearson, P.N., Palmer, M.R., 2000. Atmospheric carbon dioxide concentrations over the past 60 million years.
921 *Nature* 406, 695–699.
- 922 Pereda Suberbiola, X., Bardet, N., Iarochène, M., Bouya, B., Amaghaz, M., 2004. The first record of a sauropod
923 dinosaur from the Late Cretaceous phosphates of Morocco. *Journal of African Earth Sciences* 40, 81–88.
- 924 Picard, P., Lécuyer, C., Barrat, J.-A., Garcia, J.-P., Dromart, G., Sheppard, S.M.F., 2002. Rare earth element
925 contents of Jurassic fish and reptile teeth and their potential relation to seawater composition (Anglo-
926 Paris Basin, France and England). *Chem. Geol.* 186, 1–16.
- 927 Pin, C., Briot, D., Bassin, C., Poitrasson, F., 1994. Concomitant separation of strontium and samarium–
928 neodymium for isotopic analysis in silicate samples, based on specific extraction chromatography. *Anal.*
929 *Chim. Acta* 298, 209–217.
- 930 Rauscher, R., 1985. Les dinokystes, des outils stratigraphiques pour les séries phosphatées. Application aux
931 phosphorides du Maroc. *Sci. Géol. Bull.* 77, 69–74.
- 932 Reynard, B., Balter, V., 2014. Trace elements and their isotopes in bones and teeth: Diet, environments,
933 diagenesis, and dating of archeological and paleontological samples. *Palaeogeogr. Palaeoclimatol.*
934 *Palaeoecol.* 416, 4–16
- 935 Reynard, B., Lécuyer, C., Grandjean, P., 1999. Crystal–chemical controls on rare earth element concentrations
936 in fossil biogenic apatites and implications for paleoenvironmental reconstructions. *Chem. Geol.* 155,
937 233–241.
- 938 Schubert, A.B., Jahren, A.H., 2012. The effect of atmospheric CO₂ concentration on carbon isotope
939 fractionation in C₃ land plants. *Geochimica et Cosmochimica Acta* 96, 29–43.
- 940 Secord, R., Wing, L.S., Chew, A., 2008. Stable Isotopes in Early Eocene Mammals as Indicators of Forest Canopy
941 Structure and Resource Partitioning. *Paleobiology*, 34(2), 282–300.
- 942 Shields, G.A., Webb, G.E., 2004. Has the REE composition of seawater changed over geologic time. *Chem. Geol.*
943 204, 103–107.
- 944 Simmer, J.P., Hu, Y., Lertlam, R., Yamakoshi, Y., Hu, J.C.C., 2009. Hypomaturation enamel defects in Klk4
945 knockout/LacZ knockin mice. *J Biol Chem* 284, 19110–19121.
- 946 Snedden, J.W., Liu, C., 2010. A compilation of Phanerozoic sea level change, coastal onlaps, and recommended
947 sequence designations: AAPG Search and Discovery article 40594,
948 http://www.searchanddiscovery.net/documents/2010/40594snedden/ndx_snedden.pdf (accessed
949 October 2020)
- 950 Soncini, M.-J., 1990. Palynologie des phosphates des Oulad Abdoun (Maroc). Biostratigraphie et
951 environnements de lab phosphatogénèse dans le cadre de la crise Crétacé/Tertiaire. Université Louis
952 Pasteur, Strasbourg, p. 243. Ph.D. thesis.
- 953 Staron, R.M., Grandstaff, B.S., Gallagher, W.B., Grandstaff, D.E., 2001. REE signatures in vertebrate fossils from
954 Sewell, NJ: implications for location of the K–T boundary. *Palaios* 16, 255–265.
- 955 Suarez, C.A., Macpherson, G.L., González, L.A., Grandstaff, D.E., 2010. Heterogeneous rare earth element (REE)
956 patterns and concentrations in a fossil bone: implications for the use of REE in vertebrate taphonomy
957 and fossilisation history. *Geochim. Cosmochim. Acta* 74, 2970–2988.
- 958 Trueman, C.N., Tuross, N., 2002. Trace elements in recent and fossil bone apatite. In: Kohn, M.J., Rakovan, J.,
959 Hughes, J.M. (Eds.), *Phosphates: Geochemical, Geobiological, and Materials Importance*. Review in
960 *Mineralogy and Geochemistry* vol. 48, pp. 489–521.
- 961 Trueman, C.N., Benton, M.J., Palmer, M.R., 2003. Geochemical taphonomy of shallow marine vertebrate
962 assemblages. *Palaeogeogr. Palaeoclimatol. Palaeoecol.* 197, 151–169.

963 Trueman, C.N., Kocsis, L., Palmer, M.R., Dewdney, C., 2011. Fractionation of rare earth elements within bone
 964 mineral: a natural cation exchange system. *Palaeogeogr. Palaeoclimatol. Palaeoecol.* 310, 124–132.
 965 Tütken, T., Vennemann, W.T., Janz, H., Heizmann, E.P.J. 2006. Palaeoenvironment and palaeoclimate of the
 966 Middle Miocene lake in the Steinheim basin, SW Germany: A reconstruction from C, O, and Sr isotopes
 967 of fossil remains. *Palaeogeography, Palaeoclimatology, Palaeoecology* 241, 457–491.
 968 Tütken, T., Vennemann, T.W., Pfretzschner, H.-U., 2008. Early diagenesis of bone and tooth apatite in fluvial
 969 and marine settings: constraints from combined oxygen isotope, nitrogen and REE analysis.
 970 *Palaeogeogr. Palaeoclimatol. Palaeoecol.* 266, 254–268.
 971 Tütken, T., 2014. Isotope compositions (C, O, Sr, Nd) of vertebrate fossils from the Middle Eocene oil shale of
 972 Messel, Germany: Implications for their taphonomy and palaeoenvironment. *Palaeogeography,*
 973 *Palaeoclimatology, Palaeoecology* 416, 92–109
 974 Vail, P.R., Audemard, E., Bowman, S.A., Eisner, P.N., Perez-Crus, C., 1991. The stratigraphic signatures of
 975 tectonics, eustasy and sedimentology—an overview, in Einsele, G., Ricken, W., and Seilacher, A., eds.,
 976 *Cycles and events in stratigraphy: Springer-Verlag, Berlin*, p. 617–659.
 977 van der Meer, D.G., van den Berg van Saparoea, A.P., van Hinsbergen, D., van de Weg, R., Godderis, Y., Le Hir,
 978 G., Donnadieu, Y., 2017. Reconstructing first-order changes in sea level during the Phanerozoic and
 979 Neoproterozoic using strontium isotopes: *Gondwana Research* 44, 22–34.
 980 van Hinsbergen, D.J.J., de Groot, L.V., van Schaik, S.J., Spakman, W., Bijl, P.K., Sluijs, A., Langereis, C.G.,
 981 Brinkhuis, H., 2015. A paleolatitude calculator for paleoclimate studies. *PLoS ONE* 10, e0126946–21.
 982 <http://dx.doi.org/10.1371/journal.pone.0126946>
 983 Wei, L., Yan, C., Ye, B., Guo, X., 2008. Effects of Salinity on Leaf $\delta^{13}\text{C}$ in Three Dominant Mangrove Species
 984 along Salinity Gradients in an Estuarine Wetland, Southeast China. *J. of Coastal Research*, 241, 267–272.
 985 White, W.M., 1998. The Ocean as a Chemical system. *Geochemistry, an on-line textbook*, vol. 15. pp 645–701.
 986 Yans, J., Amaghazaz, M., Bouya, B., Cappetta, H., Iacumin, P., Kocsis, L., Mouflih, M., Selloum, O., Sen, S.,
 987 Storme1, J.-Y., Gheerbrant, E., 2014. First carbon isotope chemostratigraphy of the Ouled Abdoun
 988 phosphate Basin, Morocco; implications for dating and evolution of earliest African placental mammals.
 989 *Gondwana Research* 25, 257–269.
 990 Zazzo, A., Lécuyer, C., Mariotti, A., 2004. Experimentally-controlled carbon and oxygen isotope exchange
 991 between bioapatites and water under inorganic and microbially-mediated conditions: *Geochimica et*
 992 *Cosmochimica Acta* 68, 1–12, doi:10.1016/S0016-7037(03)00278-3.
 993 Žigaitė, Ž., Fadel, A., Blom, H., Pérez-Huerta, A., Jeffries, T., Märss, T., Ahlberg, P.E., 2016. Palaeoenvironments
 994 revealed from rare earth element systematics in vertebrate bioapatite from the Lower Devonian of
 995 Svalbard. In: Melchin, M., Jisou, J. (Eds.), *Canadian Journal of Earth Sciences*, vol. 53. pp. 788–794 8.
 996 Žigaitė, Ž., Qvarnström, M., Bancroft, A., Pérez-Huerta, A., Blom, H., Ahlberg, P.E., 2020. Trace and rare earth
 997 element compositions of Silurian conodonts from the Vesiku Bone Bed: Histological and
 998 palaeoenvironmental implications. *Palaeogeography, Palaeoclimatology, Palaeoecology* 549 109449.
 999

1001 **Figure captions**

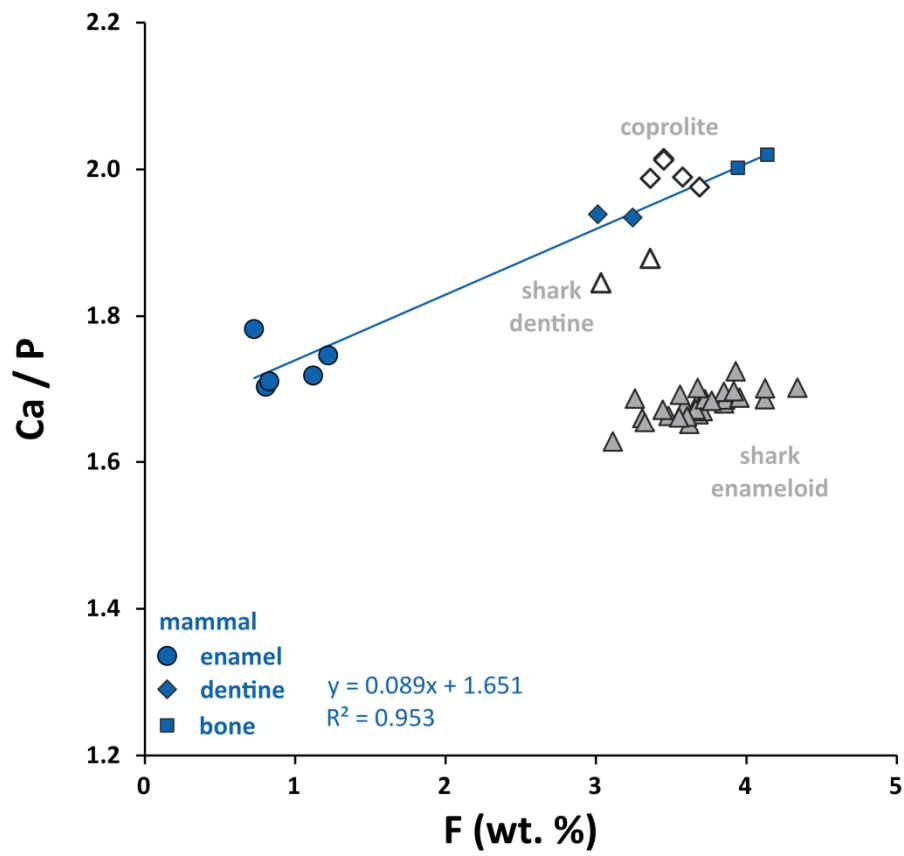
1002 **Figure 1 (a)** The origins of the fossils from the Ouled Abdoun Basin in Morocco studied here.
 1003 Quarries in the Sidi Daoui and Sidi Chennane (grey boxes) are the regions from which most
 1004 of the remains were reported. The background geochemical data are also derived here (see
 1005 **Figure 5**). **(b)** Generalized stratigraphic log of the Ouled Abdoun Basin. Note the major bone
 1006 beds and the mammal-bearing layers, however, many specimens were obtained without an
 1007 exact stratigraphic position. Abbreviation: BCbb – big coprolite bone bed. **(c)** Examples of
 1008 some of the mammals found in the Ouled Abdoun phosphate series, successively from
 1009 lowermost to uppermost levels: *Eritherium azzouzorom* (skull rostrum with teeth in ventral
 1010 view; [Gheerbrant, 2009](#)), the earliest known proboscidean, lower bone bed of bed IIa,
 1011 Selandian; *Phosphatherium escuilliei* (skull in ventral view; [Gheerbrant et al., 2005](#)), early
 1012 proboscidean, intercalary beds II/I, early Ypresian; *Daouitherium rebouli* (lower jaw ML
 1013 20269987 in lateral view), the first large proboscidean ([Gheerbrant et al., 2002](#)), upper
 1014 phosphates levels (bed 0?), middle Ypresian; *Stylolophus major* (maxillary with teeth;
 1015 [Gheerbrant et al., 2018, 2020](#)), earliest known embrithopod with *S. minor*, uppermost
 1016 phosphates levels, bed 0 or sillons, middle Ypresian.



1017

1018

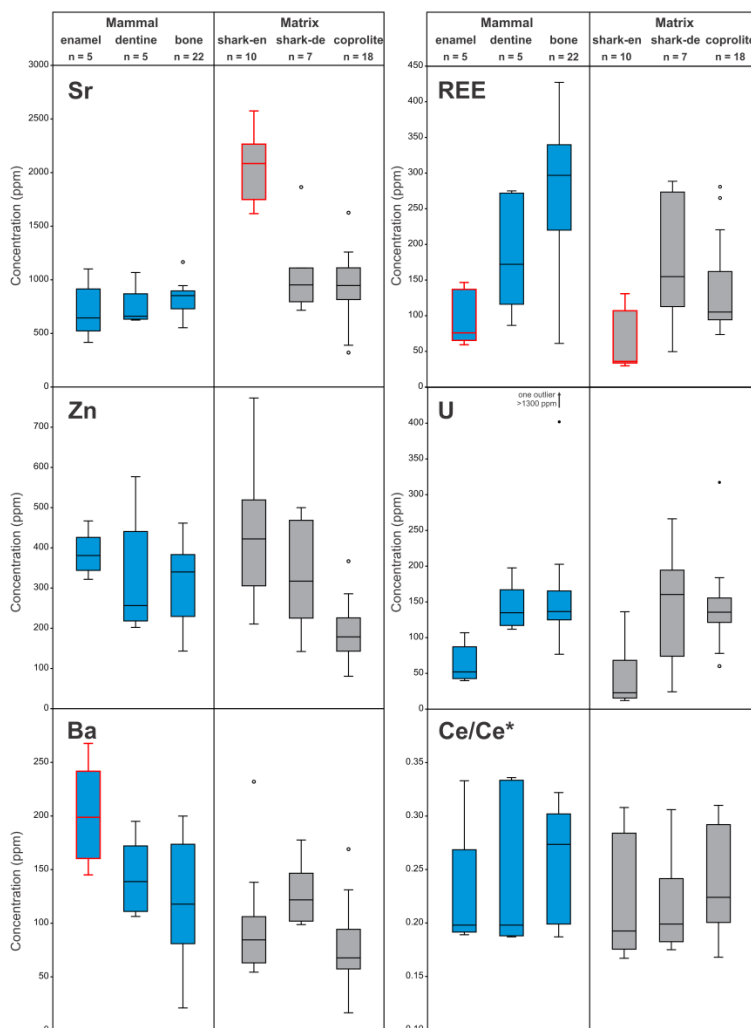
1019 **Figure 2** Major element compositions of selected mammals, shark teeth and coprolites from
1020 the Ouled Abdoun Basin.



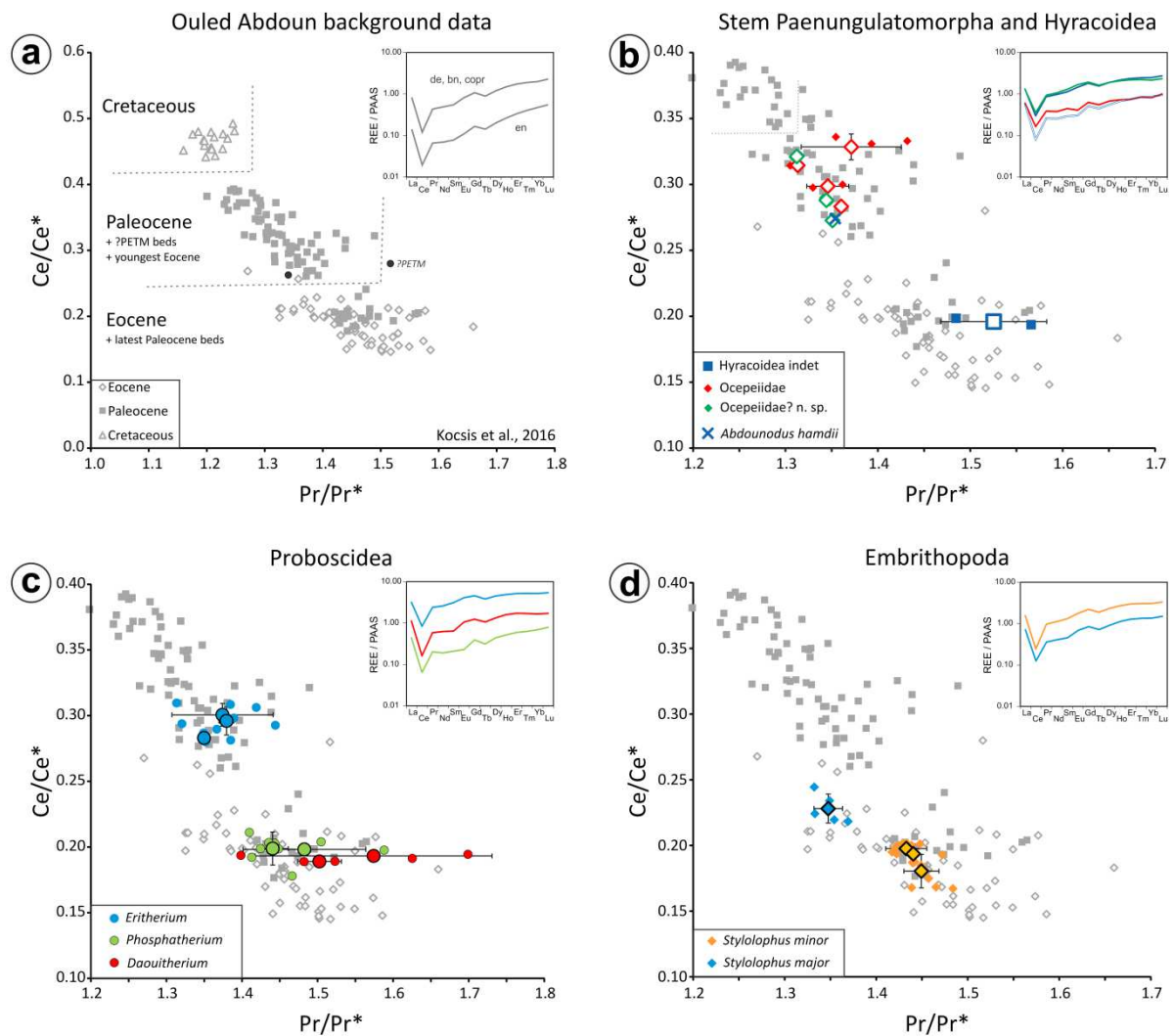
1021

1022

1023 **Figure 3** Boxplots of selected trace elements. The label “Mammal” reflects data directly
 1024 analyzed from the mammal remains (tooth enamel, dentine, and bone), while the label
 1025 “Matrix” refers to data from fossils derived from the sediment matrix (shark tooth
 1026 enameloid, dentine, and coprolite) related to the mammals. Student’s t-tests were
 1027 performed to check for statistical differences among these groups (Supplementary Material
 1028 Table-4). Note that, Sr content in shark tooth enameloid and Ba content in mammal enamel
 1029 are significantly higher than in the rest of the materials (marked red). Zinc concentration is
 1030 the highest in enamel and enameloid, and both differ significantly from the coprolite data,
 1031 whereas shark tooth enameloid is also statistically dissimilar from the dentine and bone
 1032 data. The REE concentration is the lowest in the enamel/enameloid with significant
 1033 differences from the other materials (marked red). Distribution of U content among the
 1034 materials mimics more or less that of the REEs, however with various significances among
 1035 the different groups (see Supplementary Material Table-4). The Ce/Ce* data yielded no
 1036 statistical differences among the groups.



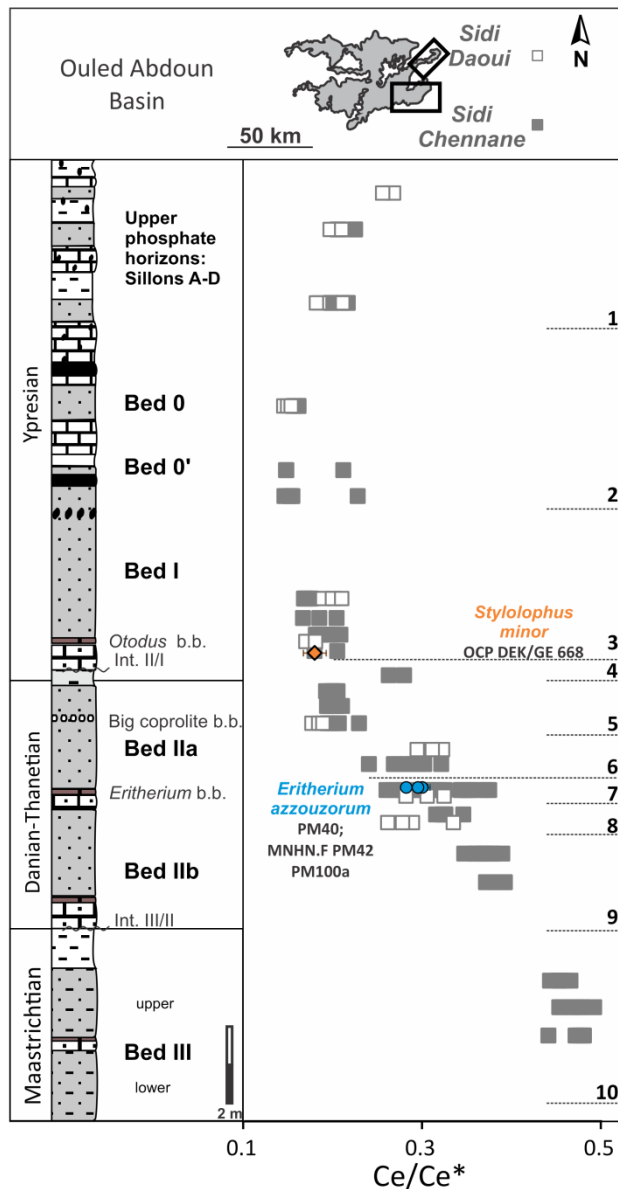
1038 **Figure 4** Ce/Ce* and Pr/Pr* variations among the samples. **(a)** Background data from the
 1039 Ouled Abdoun Basin derived from fish teeth, bones and coprolites (Kocsis et al., 2016). Note
 1040 the time-wise trending of the samples in the basin. The few overlapping samples show
 1041 meaningful stratigraphic separation, see Figure 5. **(b-d)** Comparisons of the Paleocene and
 1042 Eocene background data with the various mammal groups being investigated. Note that the
 1043 samples are better separated by Ce/Ce* than by Pr/Pr*. Inset figures display examples of
 1044 PAAS normalized REE patterns. Note the similarities in the REE distributions among the
 1045 various materials (a) and taxa (b-d).



1046

1047

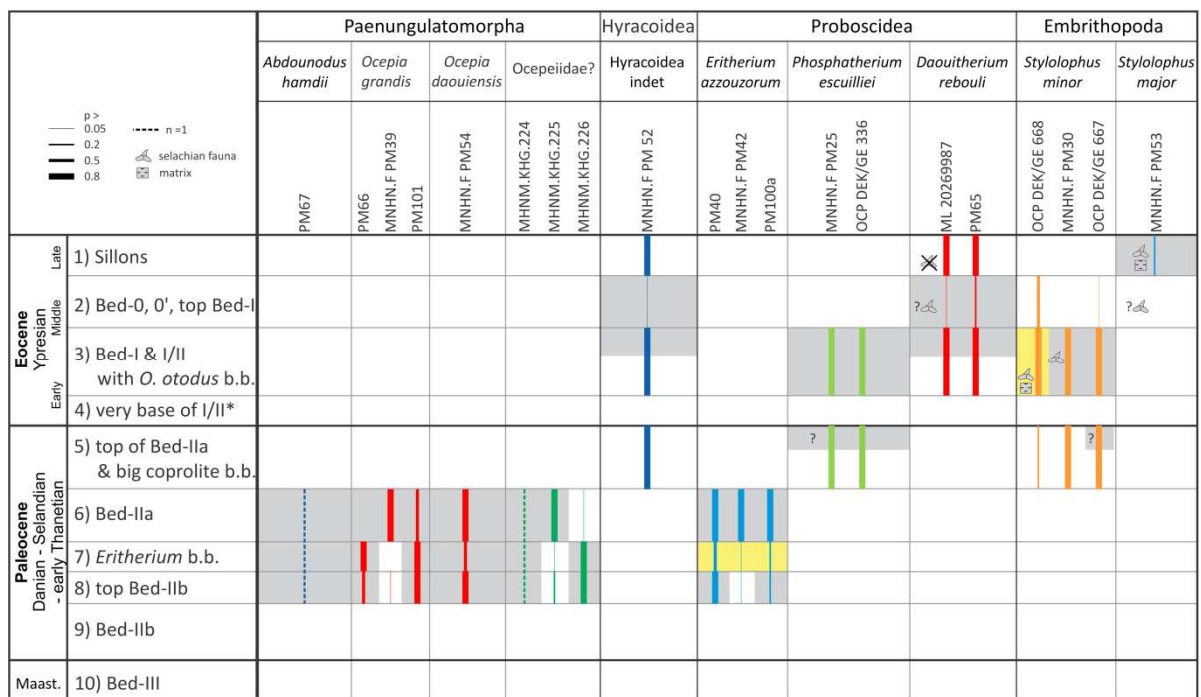
1048 **Figure 5** Stratigraphic variation of Ce/Ce* in the Ouled Abdoun Basin based on [Kocsis et al.](#)
 1049 [\(2016\)](#) and new data provided in Supplementary Material Table-1. Note that the data are
 1050 derived from two quarrying areas: Sidi Daoui and Sidi Chennane. Based on the variation of
 1051 the Ce/Ce* values the section is divided into 10 horizons (see text and Table 3). Int. III/II and
 1052 Int. II/I refer to intercalary beds respectively between Bed III and II, and, Bed II and I. Note
 1053 that the Ce/Ce* data for the few mammal remains (*S. minor* and *E. azzouzorum*) with known
 1054 stratigraphic origins fit well with the background dataset.



1055

1056

1057 **Figure 6** Stratigraphic origins of the mammal remains from the Ouled Abdoun Basin studied
 1058 here, inferred from comparisons of their mean Ce/Ce* ratios with the average stratigraphic
 1059 values of the 10 chemostratigraphic horizons (see also **Table 3**). Note that the thickness of
 1060 the lines reflects different probabilities. Where only one specimen was analyzed a dashed
 1061 line is used. In some cases, the composition of the sediment matrix and the selachian fauna
 1062 (i.e., sharks and rays) give further clue about the possible provenance. The vertical
 1063 extension of the bar across several levels for some species does not necessarily indicate a
 1064 wide stratigraphic range, but the best probability of their stratigraphic origin following the
 1065 Ce/Ce* chemostratigraphy. However, when other factors (e.g., the sedimentary matrix and
 1066 related fauna) are considered, their provenance can be reduced further, as indicated by the
 1067 grey background. The yellow background is used for those fossils whose stratigraphic origin
 1068 was known previously (see **Figure 5**).

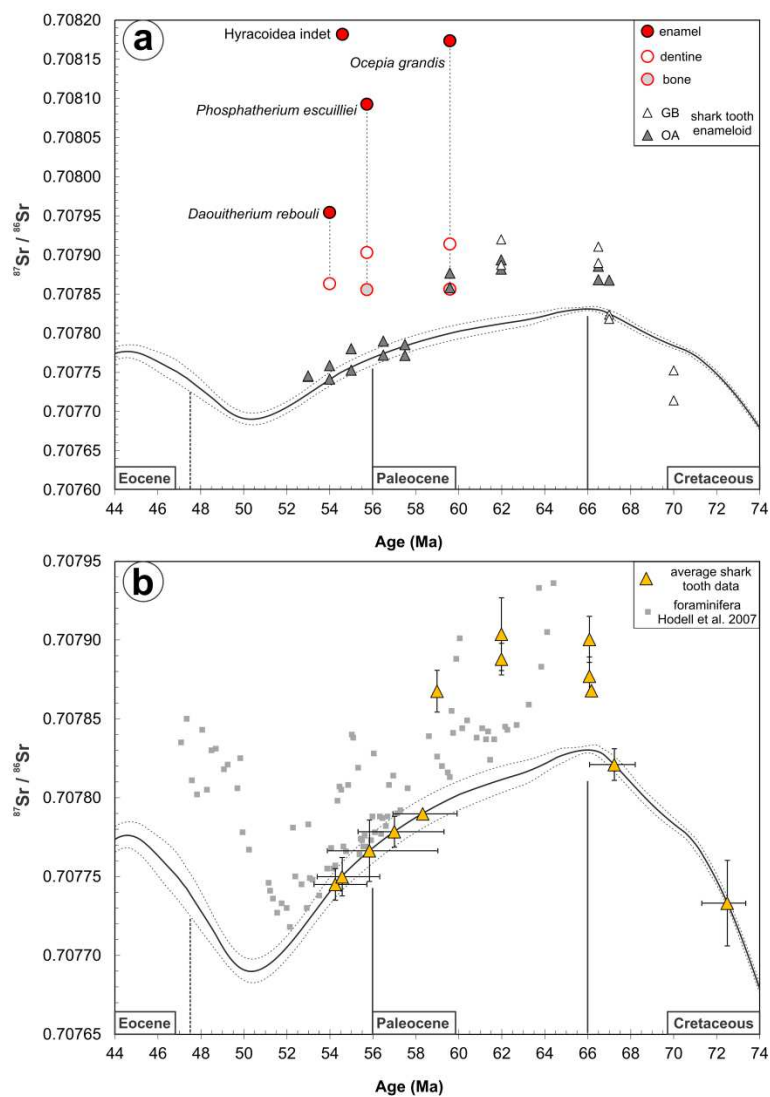


*possibly reflect reworked element from older Paleocene

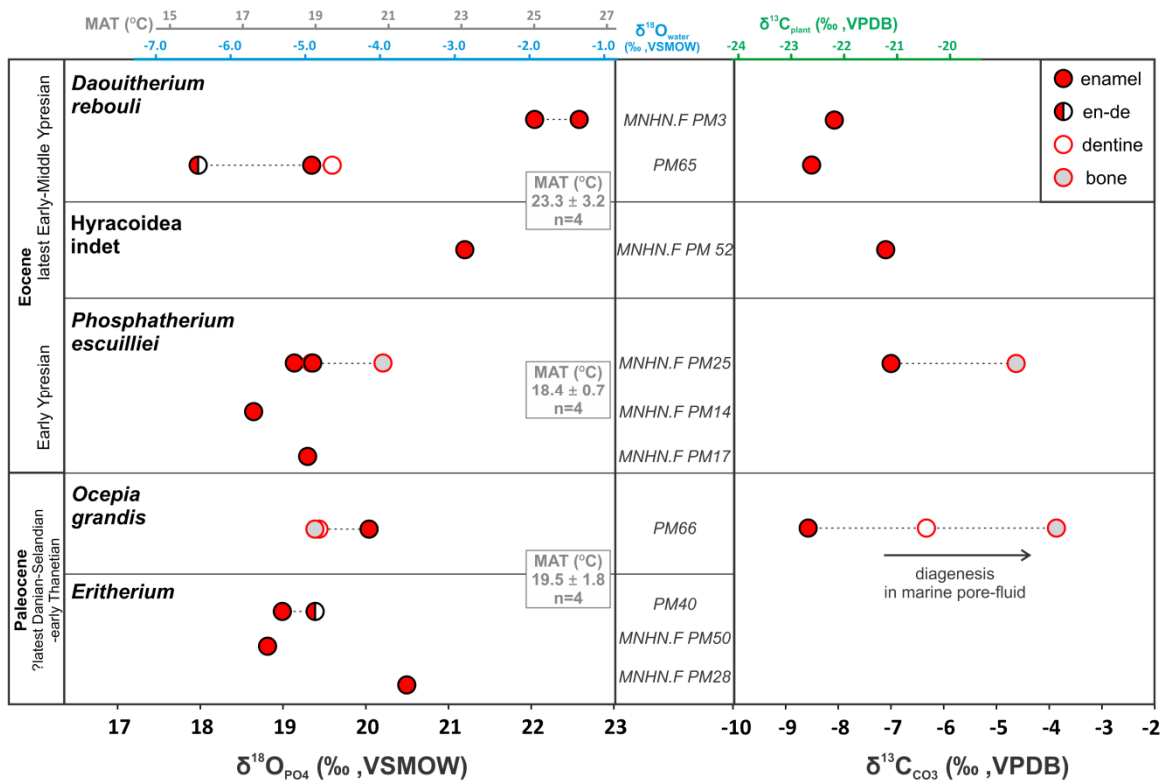
1069

1070

1071 **Figure 7** Strontium isotope variation and its comparison with the global Sr-evolution curve
 1072 ([McArthur et al., 2020](#)). Dashed lines represent the 95% confidence limits. **(a)** Mammal
 1073 samples with circles. Note that these data are well above the open ocean Sr-evolution curve
 1074 and the $^{87}\text{Sr}/^{86}\text{Sr}$ ratios decrease from enamel to bone. The enamel end-members could
 1075 reflect *in-vivo* Sr ratios, while the dentine and bone show various interactions with
 1076 seawater. Triangles are individual shark tooth enameloid analyses from the Ouled Abdoun
 1077 (OA) and Ganntour (GB) basins. The data are plotted according to stratigraphic occurrence
 1078 and predicted ages (see Supplementary material Table-5). **(b)** Layer averaged $^{87}\text{Sr}/^{86}\text{Sr}$ ratios
 1079 of shark tooth enameloid from the previous graph for the phosphate series (triangles) and
 1080 foraminifera Sr-isotope data from [Hodell et al. \(2007\)](#). The average data are plotted
 1081 according to ages derived from [McArthur et al. \(2020\)](#). Note that the latest Cretaceous and
 1082 most of the Paleocene are above the Sr-evolution curve.



1084 **Figure 8** Stable isotope compositions of selected mammal taxa and related ecological and
 1085 environmental parameters. **(a)** Oxygen isotopic composition of phosphate. The derived
 1086 isotopic composition of the ingested water and the mean annual temperature (MAT) are
 1087 calculated based on [Amiot et al. \(2004\)](#). **(b)** Carbon isotopic composition of the structural
 1088 carbonate and the calculated plant diet isotopic composition after [Kohn and Cerling \(2002\)](#).
 1089 Note the increasing trend from enamel to bone, indicating an alteration in the presence of
 1090 seawater.



1091

1092

1093 **Table captions**

1094 **Table 1** The mammal remains investigated, and related analyses. Note the uncertain
 1095 stratigraphic origin, column Locality/Layers, indicated by question marks. Abbreviations: en
 1096 – enamel, de – dentine, th – tooth, sh – shark tooth, ra – ray tooth, copr – coprolite, pel –
 1097 pellets.

Inventory No.	Order	Family	Species	Locality / Layer	Age	ICP-REE		No.	$\delta^{18}\text{O}_{\text{PO}_4}$	$\delta^{13}\text{C}-\delta^{18}\text{O}_{\text{CO}_3}$	$^{87}\text{Sr}/^{86}\text{Sr}$	EMPA	References
						specimen	matrix						
MNHN.F PM3	Proboscidea	Numidotheriidae?	<i>Daouitherium rebouli</i>	above C1?	Ypresian	-	-	-	+	+			Gheerbrant et al., 2012
PM65	Proboscidea	Numidotheriidae?	<i>Daouitherium cf. rebouli</i>	above C1?	Ypresian	en, de	-	2	+	+	+	+	Gheerbrant et al., 2012
ML 20269987	Proboscidea	Numidotheriidae?	<i>Daouitherium rebouli</i>	CO? (selachians)	Ypresian	-	-	3					
MNHN.F PM 52	Hyracoidea	indet	Hyracoidea indet	?	?Ypresian	en, de	-	2	+	+	+	+	unpublished
MNHN.F PM53	Embrithopoda	Stylophoridae	<i>Stylophus major</i>	sillons?	Ypresian	en & de	sh (en-de), copr	2 + 3					Gheerbrant et al., in press
MNHN.F PM30	Embrithopoda	Stylophoridae	<i>Stylophus minor</i>	intercalary II/I?	Ypresian	bn	sh, copr	3 + 2					Gheerbrant et al., 2018
OCF DEK/GE 667	Embrithopoda	Stylophoridae	<i>Stylophus minor</i>	intercalary II/I?	Ypresian	bn	copr	3 + 2					Gheerbrant et al., 2018
OCF DEK/GE 668	Embrithopoda	Stylophoridae	<i>Stylophus minor</i>	Otodus bonebed, intercalary II/I	Ypresian	bn, th	sh (en-de), copr	2 + 6					Gheerbrant et al., 2018
MNHN.F PM25	Proboscidea	Phosphatheriidae	<i>Phosphatherium escuillei</i>	?	Ypresian	en, de, bn	sh	3 + 1	+	+	+	+	Gheerbrant et al., 2005
OCF DEK/GE 336	Proboscidea	Phosphatheriidae	<i>Phosphatherium escuillei</i>	?	Ypresian	-	sh (en-de), ra, copr	4					Gheerbrant et al., 2005
MNHN.F PM14	Proboscidea	Phosphatheriidae	<i>Phosphatherium escuillei</i>	intercalary II/I	Ypresian	-	-	-	+				Gheerbrant et al., 2005
MNHN.F PM17	Proboscidea	Phosphatheriidae	<i>Phosphatherium escuillei</i>	intercalary II/I	Ypresian	-	-	-	+				Gheerbrant et al., 2005
PM67	Paenungulatomorpha	indet	<i>Abdounodus hamdii</i>	?	Paleocene	bn	-	1					Gheerbrant 2010
PM66	Paenungulatomorpha	Ocepeidae	<i>Ocepia grandis</i>	?Clla, 7big coprolite bone bed	Paleocene	en, de, bn	-	4	+	+	+	+	Gheerbrant et al., 2014
MNHN.F PM39	Paenungulatomorpha	Ocepeidae	<i>Ocepia grandis</i>	?	Paleocene	bn	-	2					Gheerbrant et al., 2014
PM101	Paenungulatomorpha	Ocepeidae	<i>Ocepia grandis</i>	?	Paleocene	bn	-	2					unpublished
MNHN.F PM54	Paenungulatomorpha	Ocepeidae	<i>O. daouiensis</i>	?	Paleocene	-	copr. pell	2					Gheerbrant et al., 2014
MHNM.KHG.224	Paenungulatomorpha	Ocepeidae?	n. sp.	?	Paleocene	bn	-	1					unpublished
MHNM.KHG.225	Paenungulatomorpha	Ocepeidae?	n. sp.	?	Paleocene	bn	-	2					unpublished
MHNM.KHG.226	Paenungulatomorpha	Ocepeidae?	n. sp.	?	Paleocene	bn	-	2					unpublished
PM40	Proboscidea	indet.	<i>Eritherium azzouzorum</i>	<i>Eritherium</i> bone bed	Paleocene	-	sh (en-de), copr	4	+				Gheerbrant et al., 2012
MNHN.F PM50	Proboscidea	indet.	<i>Eritherium azzouzorum</i> (juvenile)	<i>Eritherium</i> bone bed	Paleocene	-	-	-	+				Gheerbrant et al., 2012
OCF DEK/GE 498	Proboscidea	indet.	<i>cf. Eritherium sp.</i>	<i>Eritherium</i> bone bed	Paleocene	-	-	-					unpublished
MNHN.F PM28	Proboscidea	indet.	<i>Eritherium azzouzorum</i>	<i>Eritherium</i> bone bed	Paleocene	-	-	-	+				Gheerbrant et al., 2012
MNHN.F PM42	Proboscidea	indet.	<i>Eritherium azzouzorum</i>	<i>Eritherium</i> bone bed	Paleocene	-	copr	3					Gheerbrant et al., 2012
PM100a	Proboscidea	indet.	<i>Eritherium azzouzorum</i>	<i>Eritherium</i> bone bed	Paleocene	bn	sh (en), copr	1 + 4					unpublished

1098

1099

1100

1101 **Table 2** Major element, Sr-isotope ratios, and stable oxygen and carbon isotopic

1102 compositions of selected mammal specimens. Abbreviations: en – enamel, de – dentine, en-
 1103 de – enamel dentine transition.

No.	Species	Material	CaO (wt%)	P ₂ O ₅ (wt%)	F (wt%)	Ca/P	n	$^{87}\text{Sr}/^{86}\text{Sr}$	1SE x10 ⁻⁶	Ma	$\delta^{18}\text{O}_{\text{PO}_4}$ VSMOW	std.	Specimen average	std.	Taxon average	std.	$\delta^{13}\text{C}_{\text{VPOB}}$	std.	$\delta^{18}\text{O}_{\text{VPOB}}$	$\delta^{18}\text{O}_{\text{VSMOW}}$	std.	Yield (%)	
MNHN.F PM3	<i>Daouitherium rebouli</i>	right m3	en								22.0	0.1											
			en								22.6	0.2	22.3	0.4									
PM65	<i>Daouitherium rebouli</i>	dP2-4 and M1	en	51.7	36.7	0.73	1.78	3	0.707954	3	54	19.3	0.1										
			en-de	50.2	37.0	1.12	1.72	1				18.0	0.1										
			de	45.1	29.5	3.01	1.94	3	0.707863	3	54	19.6	0.2	19.0	0.9	20.6	2.4						
MNHN.F PM 52	Hyracoidea indet	m3	en	50.3	37.2	0.83	1.71	3	0.708182	3	58	21.2	0.1	21.2	0.3	21.2							
MNHN.F PM25	<i>Phosphatherium escuillei</i>	right p3	en	52.1	38.7	0.81	1.70	3	0.708093	5	56.5	19.4	0.1										
			de	49.4	31.2	3.95	2.00	2	0.707903	3	56.5	19.3	0.2										
		right m1	en								19.1	0.1											
		jaw frg.	bone	50.0	31.3	4.14	2.02	2	0.707856	3	56.5	20.2	0.0	19.5	0.5								
MNHN.F PM14	<i>Phosphatherium escuillei</i>	m3	en								18.6	0.2	18.6	0.3									
MNHN.F PM17	<i>Phosphatherium escuillei</i>	right M2	en								19.3	0.3	19.3	0.3	19.2	0.5							
PM66	<i>Ocepia grandis</i>	tooth fragment	en	50.3	36.5	1.22	1.75	2	0.708174	3	58	20.0	0.0										
			de	48.9	32.0	3.25	1.93	2	0.707914	4	58	19.4	0.0										
		bone fragment	bone						0.707856	3	58	19.4	0.3	19.6	0.4	19.6	0.4						
PM40	<i>Eritherium</i>	m1	en								19.0												
			en-de								19.4	0.2	19.2	0.3									
MNHN.F PM50	<i>Eritherium</i>	p2	en								18.8	0.3	18.8	0.3									
MNHN.F PM28	<i>Eritherium</i>	en	en								20.5	0.1	20.5	0.3	19.5	0.9							

1104

1105

1106

1107 **Table 3** Tukey’s pairwise tests comparing the samples separately with designated horizons.

1108 In the case of Eocene mammals Horizons 1-5, while for the Paleocene taxa Horizons 5-10

1109 were used. Note that only the probability values are listed. Layers with highlighted values

1110 could be considered as a possible provenance for the given mammal fossils, while the

1111 strikethrough numbers indicate invalid scenarios. See also text and **Figure 6**.

Eocene mammals												
Tukey's pairwise test		MNHN.F PM53	OCF DEK/GE 668	MNHN.F PM30	OCF DEK/GE 667	MNHN.F PM25	OCF DEK/GE 336	ML 20269987	PM65	MNHN.F PM 52		
p (same) relative to the horizons (1-5)		<i>S. major</i>	<i>S. minor</i>	<i>S. minor</i>	<i>S. minor</i>	<i>P. escuillei</i>	<i>P. escuillei</i>	<i>D. rebouli</i>	<i>D. rebouli</i>	Hyracoidea indet		
H. Age	Beds	n	5	8	5	5	4	5	3	2		
1	late Ypresian	Sillons	22	0.30	0.19	0.98	0.90	0.99	0.99	0.92	0.81	0.98
2	latest Early - Middle Ypresian	Bed 0-0' & Top Bed I	14	< 0.05	0.56	< 0.05	0.07	< 0.05	< 0.05	0.12	0.34	0.12
3	early Ypresian	Bed-I & I/II	23	< 0.05	0.99	0.93	0.99	0.92	0.90	1.00	1.00	0.98
4	?PETM	base I/II	2	< 0.05	< 0.05	< 0.05	< 0.05	< 0.05	< 0.05	< 0.05	< 0.05	< 0.05
5	late Thanetian	Top Bed III & Big Copr Bed	18	0.10	0.47	1.00	1.00	1.00	1.00	1.00	0.97	1.00

Paleocene mammals											
Tukey's pairwise test		PM40	MNHN.F PM42	PM100a	PM66	MNHN.F PM39	PM101	MNHN.F PM54	MHNM.KHG.225	MHNM.KHG.226	
p (same) relative to the horizons (5-10)		<i>E. azzouorum</i>	<i>E. azzouorum</i>	<i>E. azzouorum</i>	<i>O. grandis</i>	<i>O. grandis</i>	<i>O. grandis</i>	<i>O. daouiensis</i>	<i>O. daouiensis</i>	<i>O. daouiensis</i>	
H. age	Beds	n	4	3	5	4	2	2	2	2	
5	late Thanetian	Top Bed-III & Big Copr Bed	18	< 0.05	< 0.05	< 0.05	< 0.05	< 0.05	< 0.05	< 0.05	< 0.05
6	Selandian-early Thanetian	Bed-IIa	10	0.99	0.96	1.00	< 0.05	0.98	0.53	1.00	1.00
7	Selandian-early Thanetian	Eritherium bone bed	30	0.49	< 0.05	0.17	0.96	< 0.05	1.00	0.59	0.11
8	Early Selandian-latest Danian	top Bed-IIb	11	0.85	0.06	0.49	0.73	0.14	1.00	0.87	0.30
9	earliest Selandian-late Danian	Bed-IIb	15	< 0.05	< 0.05	< 0.05	< 0.05	< 0.05	< 0.05	< 0.05	< 0.05
10	latest Maastrichtian	Bed-III	18	< 0.05	< 0.05	< 0.05	< 0.05	< 0.05	< 0.05	< 0.05	< 0.05

1112

1113 **Table 4** Tukey’s pairwise tests among the Eocene and Paleocene mammal samples. Note

1114 that *S. major* is completely different from the rest of the Eocene fossils, while among the

1115 Paleocene samples some of the Ocepeiidae spp. (e.g., PM66 & MHNM.KHG.226) are

1116 somewhat different from the rest.

Eocene mammals										
Tukey's pairwise test	MNHN.F PM53	OCF DEK/GE 668	MNHN.F PM30	OCF DEK/GE 667	MNHN.F PM25	OCF DEK/GE 336	ML 20269987	PM65	MNHN.F PM 52	
Q / p (same)	<i>S. major</i>	<i>S. minor</i>	<i>S. minor</i>	<i>S. minor</i>	<i>P. escuillei</i>	<i>P. escuillei</i>	<i>D. rebouli</i>	<i>D. rebouli</i>	Hyracoidea indet	
<i>S. major</i>		< 0.05	< 0.05	< 0.05	< 0.05	< 0.05	< 0.05	< 0.05	< 0.05	
<i>S. minor</i>	9.68		0.27	0.61	0.25	0.21	0.65	0.94	0.41	
<i>S. minor</i>	6.16	3.53		1.00	1.00	1.00	1.00	0.93	1.00	
<i>S. minor</i>	6.97	2.71	0.82		1.00	1.00	1.00	1.00	1.00	
<i>P. escuillei</i>	6.07	3.62	0.09	0.91		1.00	1.00	0.92	1.00	
<i>P. escuillei</i>	5.95	3.73	0.20	1.02	0.11		1.00	0.89	1.00	
<i>D. rebouli</i>	7.07	2.62	0.91	0.10	1.00	1.11		1.00	1.00	
<i>D. rebouli</i>	7.94	1.74	1.78	0.97	1.88	1.99	0.87		0.98	
Hyracoidea indet	6.52	3.16	0.37	0.45	0.46	0.57	0.54	1.42		

Paleocene mammals										
Tukey's pairwise test	PM40	MNHN.F PM42	PM100a	PM66	MNHN.F PM39	PM101	MNHN.F PM54	MHNM.KHG.225	MHNM.KHG.226	
Q / p (same)	<i>E. azzouorum</i>	<i>E. azzouorum</i>	<i>E. azzouorum</i>	<i>O. grandis</i>	<i>O. grandis</i>	<i>O. grandis</i>	<i>O. daouiensis</i>	<i>O. daouiensis</i>	<i>O. daouiensis</i>	
<i>E. azzouorum</i>		0.25	1.00	< 0.05	0.28	0.55	1.00	0.64	0.12	
<i>E. azzouorum</i>	3.70		0.63	< 0.05	1.00	< 0.05	0.36	1.00	< 0.05	
<i>Eritherium</i>	1.03	2.67		< 0.05	0.68	0.20	1.00	0.96	< 0.05	
<i>O. grandis</i>	5.78	9.48	6.81		< 0.05	0.53	< 0.05	< 0.05	0.98	
<i>O. grandis</i>	3.59	0.10	2.56	9.37		< 0.05	0.40	1.00	< 0.05	
<i>O. grandis</i>	2.86	6.56	3.90	2.92	6.46		0.40	< 0.05	0.98	
<i>O. daouiensis</i>	0.36	3.33	0.67	6.15	3.23	3.23		0.78	0.08	
<i>Ocepeiidae?</i>	2.66	1.04	1.63	8.44	0.94	5.52	2.29		0.00	
<i>Ocepeiidae?</i>	4.32	8.02	5.35	1.46	7.92	1.46	4.69	6.98		

1117

1118

1119 **Supplementary Data Tables**

1120 **SM Table 1** Supplementary trace element concentration and ratio data from Sidi Chennane
1121 and Sidi Daoui areas, focusing on some of the bone beds: the *Eritherium* bone bed (base Bed
1122 IIa), big coprolite bone bed (top Bed IIa), and *Otodus* bone bed (intercalary II/I). The Ce/Ce*
1123 and Pr/Pr*ratios are plotted in [Figures 4 and 5](#) as a part of the background dataset.

1124

1125 **SM Table 2** Major element compositions of marine remains (shark teeth, coprolites) from
1126 the Sidi Chennane quarry of the Ouled Abdoun Basin (see [Figure 2](#) in the paper).

1127

1128 **SM Table 3** Trace element concentrations, Ce/Ce* and Pr/Pr*ratios of the mammal
1129 specimens and related matrix from the Ouled Abdoun Basin investigated here (see [Figures](#)
1130 [3-5](#) in the paper).

1131

1132 **SM Table 4** Student's t-tests on selected geochemical data displayed as boxplots in [Figure 3](#).
1133 The six different types of materials studied are mammal enamel, dentine, bones, and shark
1134 tooth enameloid, dentine, and coprolites. Significant differences ($p < 0.05$) are marked red,
1135 whereas underlined data indicate unequal variances between the compared groups.

1136

1137 **SM Table 5** Strontium isotope ratios of shark tooth enameloid from the Ouled Abdoun Basin
1138 (see [Figure 7](#) in the paper). Individual analyses are plotted in [Figure 7a](#), while the average
1139 data and derived Sr-isotope ages based on [McArthur et al. \(2020\)](#) are in [Figure 7b](#).

1140

1141 **SM Table 6** Ten defined chemostratigraphic horizons and their average Ce/Ce* values and
1142 the related F and Student's t-test statistics. df- degree of freedom; p- probability.

1143 Underlined p-values for the F-test indicate significantly different variances. In this case, the
1144 Student's t-tests were performed for unequal variance. The grey p-values for the Student's
1145 t-test highlights horizon pairs for which the means of the Ce/Ce* values do not differ
1146 significantly.

1147

1148 **SM Table 7** Recovered selachian fauna and matrix data from a few mammal specimens
1149 belonging to the species *S. minor*, *S. major*, and *D. rebouli*.